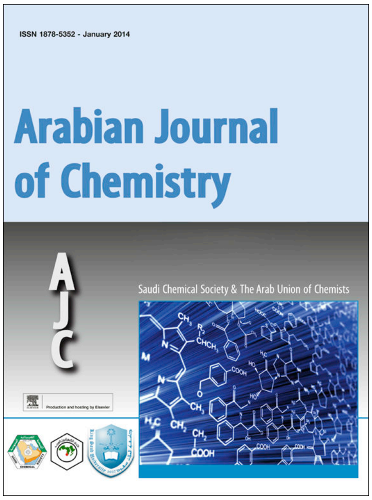

Original article

Metal Framework as a Novel Approach for the Fabrication of Electric Double Layer Capacitor Device with High Energy Density Using Plasticized Poly(vinyl alcohol): Ammonium Thiocyanate Based Polymer Electrolyte

M.A. Brza, Shujahadeen B. Aziz, H. Anuar, Fathilah Ali, M.H. Hamsan, M.F.Z. Kadir

PII: S1878-5352(20)30285-9
DOI: https://doi.org/10.1016/j.arabjc.2020.08.006
Reference: ARABJC 2763

To appear in: *Arabian Journal of Chemistry*

Received Date: 6 June 2020
Revised Date: 6 August 2020
Accepted Date: 9 August 2020

Please cite this article as: M.A. Brza, S.B. Aziz, H. Anuar, F. Ali, M.H. Hamsan, M.F.Z. Kadir, Metal Framework as a Novel Approach for the Fabrication of Electric Double Layer Capacitor Device with High Energy Density Using Plasticized Poly(vinyl alcohol): Ammonium Thiocyanate Based Polymer Electrolyte, *Arabian Journal of Chemistry* (2020), doi: https://doi.org/10.1016/j.arabjc.2020.08.006

Title page

Metal Framework as a Novel Approach for the Fabrication of Electric Double Layer Capacitor Device with High Energy Density Using Plasticized Poly(vinyl alcohol): Ammonium Thiocyanate Based Polymer Electrolyte

M. A. Brza[1], Shujahadeen B. Aziz[2,3,*], H. Anuar[1], Fathilah Ali[4], M. H. Hamsan[5] and M. F. Z. Kadir[6]

[1]Department of Manufacturing and Materials Engineering, Faculty of Engineering, International Islamic University of Malaysia, Kuala Lumpur, Gombak 53100, Malaysia
[2]Advanced Polymeric Materials Research Lab., Department of Physics, College of Science, University of Sulaimani, Qlyasan Street, Sulaimani 46001, Iraq
[3]Department of Civil Engineering, College of Engineering, Komar University of Science and Technology, Sulaimani, 46001, Kurdistan Regional Government, Iraq
[4]Department of Biotechnology Engineering, Faculty of Engineering, International Islamic University of Malaysia, Kuala Lumpur, Gombak 53100, Malaysia
[5]Institute for Advanced Studies, University of Malaya, 50603 Kuala Lumpur, Malaysia
[6]Centre for Foundation Studies in Science, University of Malaya, 50603 Kuala Lumpur, Malaysia

[*]Correspondence: shujahadeenaziz@gmail.com

Metal Framework as a Novel Approach for the Fabrication of Electric Double Layer Capacitor Device with High Energy Density Using Plasticized Poly (vinyl alcohol): Ammonium Thiocyanate Based Polymer Electrolyte

M. A. Brza[1,2], Shujahadeen B. Aziz[2,3,*], H. Anuar[1], Fathilah Ali[4], M. H. Hamsan[5], M. F. Z. Kadir[6] and Rebar T. Abdulwahid[7]

[1]Department of Manufacturing and Materials Engineering, Faculty of Engineering, International Islamic University of Malaysia, Kuala Lumpur, Gombak 53100, Malaysia.
[2]Advanced Polymeric Materials Research Lab., Department of Physics, College of Science, University of Sulaimani, Qlyasan Street, Sulaimani 46001, Iraq.
[3]Department of Civil Engineering, College of Engineering, Komar University of Science and Technology, Sulaimani, 46001, Kurdistan Regional Government, Iraq.
[4]Department of Biotechnology Engineering, Faculty of Engineering, International Islamic University of Malaysia, Kuala Lumpur, Gombak 53100, Malaysia.
[5]Institute for Advanced Studies, University of Malaya, 50603 Kuala Lumpur, Malaysia.
[6]Centre for Foundation Studies in Science, University of Malaya, 50603 Kuala Lumpur, Malaysia.
[7]Department of Physics, College of Education, University of Sulaimani, Old Campus, Kurdistan Regional Government, Sulaimani 46001, Iraq.

[*]Correspondence: shujahadeenaziz@gmail.com

Abstract

High performance electric double-layer capacitors (EDLCs) based on poly (vinyl alcohol) (PVA): ammonium thiocyanate (NH_4SCN):Cu(II)-complex plasticized with glycerol (GLY) have been fabricated. The maximum DC ionic conductivity (σ_{DC}) of 2.25×10^{-3} S cm^{-1} is achieved at ambient temperature. The X-ray diffraction (XRD) patterns confirmed that the addition of both Cu(II)–complex and GLY enhanced the amorphous region within the samples. Through the Fourier transform infrared (FTIR) the interactions between the host polymer and other components of the prepared electrolyte are observed. The FESEM images reveal that the surface morphology of the samples showed a uniform smooth surface at high GLY concentration. This is in good agreement with the XRD and FTIR results. Transference numbers of ion (t_{ion}) and electron (t_{el}) for the highest conducting composite polymer electrolyte (CPE) are recognized to be 0.971 and 0.029, respectively. The linear sweep voltammetry (LSV) revealed that the electrochemical stability window for the CPE is 2.15 V. These high values of t_{ion} and potential stability established the suitability of the synthesized systems for EDLC application. Cyclic voltammetry (CV) offered nearly rectangular shape with the lack of Faradaic peak. The specific capacitance and energy density of the EDLC are nearly constant within 1000 cycles at a current density of 0.5 mA/cm^2 with average of 155.322 F/g and 17.473 Wh/Kg, respectively. The energy density of the EDLC in the current work is in the range of battery specific energy. The EDLC performance was found to be stable over 1000 cycles. The low value of equivalent series resistance reveals that the EDLC has good electrolyte-electrode contact. The EDLC exhibited the initial high power density of 4.960×10^3 W/Kg.

Keywords: PVA polymer electrolyte; Glycerol plasticizer; Cu(II)-complex;

Electrochemical and EDLC.

1. Introduction

Supercapacitors (SCs) can be categorized into three kinds of electrochemical capacitor (EC) which are known as electric double-layer capacitor (EDLC), pseudocapacitor, and hybrid SCs. In the EDLC the electric energy is stored based on electrosorption process (charge-discharge) when the Helmholtz double layers are formed on porous electrodes through movement of ions inside the electrolyte [1]. Pseudocapacitor stores energy faradaically by chemical interaction between the electrolyte and electrode for example redox reaction. The process of charge storage used in hybrid capacitors is a mix of the both faradaic reaction and non-faradaic reaction. EDLC is the typical non-faradaic SC. The charge-discharge cycles just involve ions adsorption on the surface of the electrodes. It is promising to attain high energy density (E_d) and power density (P_d) using EDLC. [2-4]. ECs are devices which can occupy the spaces between battery and electrostatic capacitor with regard to E_d and P_d as shown in Ragone plot (see ***Figure 1***). The Ragone plot is a chart employed for comparing the performance of several energy storage devices for example SCs, fuel cells, conventional capacitors, and batteries [5]. The achieved E_d in the current work is 17.473 Wh/Kg throughout 1000 cycles which is in the range of E_d of batteries (see ***Figure 1***).

An electrolyte film and two porous electrodes are included in the EDLC device. Mostly carbon-based electrodes are used for creating these SCs [5]. The different carbon-based electrode materials used in EDLCs are carbon aerogels, activated carbon (AC), carbon nanotubes, carbon nanosize, graphites, and carbon nanofibers [6]. AC is used in this study as an electrode because of its high conductivity, chemical stability, large surface area (>1000 m^2g^{-1}), cost effective, and high porosity (>2 nm pore width) [7, 8]. At the same time, the electrolyte can be liquid electrolyte (LE), solid polymer electrolyte (SPE), gel polymer electrolyte (GPE) [9]. The SPE outweigh LE in many substantial characteristics such as electrolyte leakage, better safety, high flexibility, light weight, and excellent thermal stability [1, 10]. These features can essentially enhance the EDLC electrochemical performances. Additionally, the increased demand for flexible electronic devices resulted in an increasing trend of employing polymer hydrogels as the separators and electrolytes for flexible electrochemical energy storage devices [11]. Compared to SPE, hydrogel electrolyte consists of elastic crosslinked hydrated polymer chains that trap water in the interstitial spaces of the polymer matrices mainly by surface tension [12]. This makes the hydrogel electrolyte appear usually wet, which gives a tough and soft property to the electrolyte [12].

In recent decades, biodegradable polymers have been widely studied to be employed in the renewable energy sources and electrochemical energy storage devices to solve the environmental issues [13]. However, the electrical and mechanical properties of these polymers need enhancement in order to be used in the energy devices [13]. Various host polymers have been widely investigated in this field, such as chitosan [14], hydroxylethyl cellulose (HEC) [15], Polyethylene oxide (PEO) [16], poly(vinyl alcohol) (PVA) [17], methylcellulose (MC) [18], N, N-dimethyl acrylamide (DMA) [19], and polyacrylamide-co-acrylic acid (PAAC) [20]. Previous studies are shown that both mechanical and electrical properties of PVA can be considerable enhanced when doped with glycerol (GLY) and different salts such as calcium chloride ($CaCl_2$) and sodium chloride (NaCl) [21,22].

In this research, poly (vinyl alcohol) (PVA) was preferred as a host polymer due to its biodegradable capability, low cost, and easy processability. Ammonium thiocyanate (NH_4SCN) was used in the current study as a low lattice energy salt to deliver H^+ to the CPE system [23]. Srivastava et al. [24] have stated that the charge carrier in PEO combined with NH_4SCN is the H^+. NH_4SCN has low lattice energy of 605 $kJ.mol^{-1}$ compared to other ammonium salts, such as NH_4Br (667 kJ mol^{-1}), NH_4Cl (694.7 kJ mol^{-1}), NH_4NO_3 (648.9 kJ mol^{-1}), NH_4F (834.5 kJ mol^{-1}), NH_4I (626 kJ mol^{-1}), etc. [25, 26]. Therefore, it is possible to dissociate it easily into cations and anions when inserted in water as a solvent. This means, larger number ammonium ions are offered by NH_4SCN to the polymer. The addition of Cu(II)–complex to the polymer electrolyte (PE) was attempted to improve the performance of the electrolyte films via establishing an amorphous nature which is crucial for ion transport process. In this study, glycerol (GLY) was also chosen as an appropriate plasticizer since it enhances DC conductivity (σ_{DC}) because of the existence of three groups of hydroxyl (OH). It is believed that the high dielectric constant value (ε_r) of 42.5 for GLY can reduce the attraction force amongst the cations and anions of the salt, and also weaken the force between chains of the polymers [27, 28].

In our previous study it was revealed that the amorphous structure of PVA polymer enhanced through the inclusion of Cu(II)–complex [29]. To the best of our knowledge, no study has been reported in literature regarding the role of metal complex (e.g. Cu(II)-complex) or metal framework on EDLC performance. Mohamad & Arof, [30] have fabricated the plasticized system of PVA–KOH–Propylene carbonate (PC)–Al_2O_3. The results showed that the samples conductivity could be significantly increased with raising the PC plasticizer content [30]. Lim et al., [1] fabricated EDLC device based on AC electrodes and PVA:$LiClO_4$:TiO_2. They are noted that the insertion of TiO_2 into the PVA–$LiClO_4$ system resulted in the σ_{DC} of 1.3 × 10^{-4} S cm^{-1} and specific capacitance (C_d) value of 12.5 F g^{-1}. Nonetheless, the C_d of the CPE is still low and the addition of TiO_2 was not significantly enhanced the electrochemical performances of the EDLC. Thus, this work aims to improve the ionic conductivity and electrochemical properties of PVA based polymer electrolyte, doped with ammonium thiocyanate (NH_4SCN):Cu(II)-complex and plasticized with various amount of glycerol (GLY). Then, the highest conducting sample will be used as polymer electrolyte in the fabrication of EDLC, and the performance of the device will be explored.

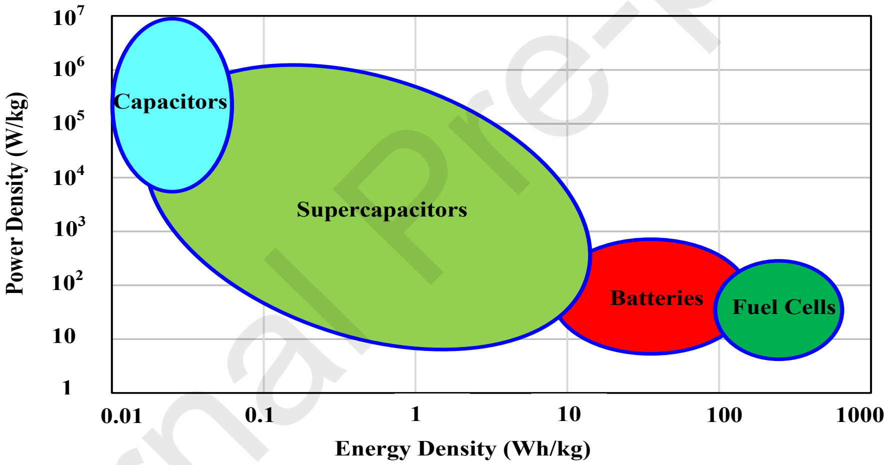

Figure 1. Ragone plot of E_d versus P_d for numerous electrochemical energy storage devices [4].

2. Materials and Methods

2.1 Materials

Sigma-Aldrich (Kuala Lumpur, Malaysia) provided poly(vinyl alcohol) (PVA) powder (average molecular weight = 85000-124000), copper(II) chloride (molecular weight = 134.45 g/mol) and GLY (molecular weight = 92.09382 g/mol). HmbG chemicals, EMPLURA, and Timcal provided ammonium thiocyanate (NH_4SCN) (molecular weight = 76.12 g/mol), N-Methyl-2-pyrrolidone (NMP) (molecular weight = 99.13 g/mol), and carbon black (molecular weight = 12.01 g/mol), respectively. Magna value delivered both of the polyvinylidene fluoride (PVdF) (average molecular weight = ~534,000 by GPC) and activated carbon (AC) (RP20) (molecular weight = 12.01 g/mol).

2.2 Electrolyte Preparation

One gram of PVA was dissolved in 40 mL of distilled water. The solution was stirred using magnetic stirrer at the temperature of 80 ^{o}C for around 60 min to prepare the PVA solution. The PVA solution was then left to cool down to room temperature. Then, fixed amount of 50 wt.% of NH_4SCN were added to the PVA solutions and stirred constantly with magnetic stirrer at ambient temperature until the salt was fully dissolved in the PVA polymer solutions. Later, PVA:NH_4SCN was included with 10 mL of Cu(II)-complex (synthesis of Cu(II)-complex was described in our previous work in materials and methods section in ref. [29]. Subsequently, the solutions were mixed and stirred to obtain a good dispersion of Cu(II)-complex in the solution. After that, the PVA:NH_4SCN:Cu(II)-complex were plasticized with 10, 20, 30, and 40 wt.% GLY and then the prepared samples were coded as PGNC-1, PGNC-2, PGNC-3, and PGNC-4, respectively. Finally, the plasticized solutions were stirred and mixed until a homogeneous solution was reached and then preserved in the plastic Petri dishes and left for drying at room temperature. For drying better, the fabricated CPE films were preserved in a dessicator comprising silica gel before characterisations.

2.3 Characterization techniques

X-Ray Diffraction (XRD) spectra were achieved through the use of Empyrean X-ray diffractometer, (PANalytical, Netherland) with operating voltage of 40×10^3 V and operating current of 40×10^{-3} A. The CPE films were scanned with a CuKα X-ray monochromatic radiation at 0.15406 nm wavelength and the 2θ glancing angle was ranged from 10° to 80° with 0.1° step size.

To study the PVA film as well as CPE films, Fourier Transform Infrared (FTIR) spectrophotometer (Thermo Scientific, Nicolet iS10) was used in the wavenumber range from 4000 to 450 cm^{-1} and with having 2 cm^{-1} resolutions.

A Hitachi SU8220 was used to conduct the field emission scanning electron microscopy (FESEM) at 500× magnification. FESEM images were taken to consider the CPE films morphology.

The pure PVA and CPE impedance spectra were accomplished using electrochemical impedance spectroscopy (EIS) [3532-50 LCR HiTESTER (HIOKI)] in the frequencies between 50 Hz and 5×10^6 Hz. The synthesized CPE films were cut for circles with 20 mm in diameter as well as located between stainless steel (SS) electrodes under pressure of a spring. The CPE samples were linked to a computer program to consider real (Z') and imaginary (Z'') parts of the complex impedance (Z^*) spectra.

2.4 Electrolyte Characterization

2.4.1 Ionic transference number Analysis

Two types transference number (TNM) were analyzed, which are ionic (t_{ion}) and electronic (t_{el}) TNM. The cell preparation arrangement was SS| highest CPE (PGNC-4)| SS. The cell was connected to a V&A Instrument DP3003 digital DC power supply and a UNI-T UT803 multimeter. The circuit diagram for the TNM measurement is shown in ***Figure 2***. The cell polarized versus time at the working voltage of 0.2 V and ambient temperature. t_{ion} and t_{el} can be calculated from Eq.s (1) and (2) [31]:

$$t_{ion} = \frac{I_i - I_{ss}}{I_i} \tag{1}$$

$$t_{el} = 1 - t_{ion} \tag{2}$$

Here initial current and steady-state current are designated as I_i and I_{ss}, correspondingly.

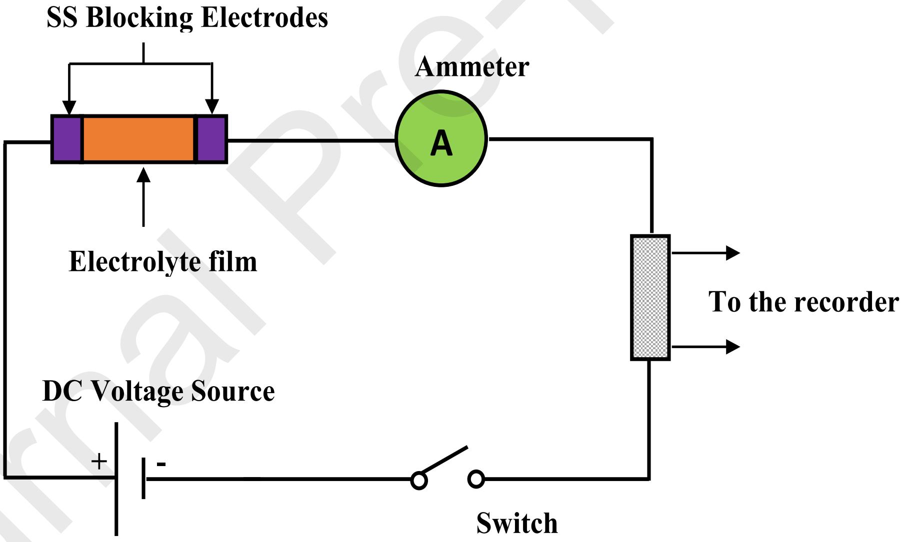

Figure 2. Illustration of TNM experimental system.

2.4.2 Linear sweep voltammetry (LSV)

In order to check the electrochemical stability of the prepared CPEs before the EDLC fabrication, the linear sweep voltammetry (LSV) investigation was accomplished. The cell arrangement for the LSV is similar to the TNM examination in ***Figure 2***. Scan rate of 10 mV s^{-1} was given from 0 to 2.5 V at ambient temperature. The cell was linked to the working electrode, reference electrode, and counter electrode by means of Digi-IVY DY2300 potentiostat. When potential was swept linearly between working electrode and counter electrode, the change in the current value at the working electrode was recorded. The cell setup for the LSV test is displayed in ***Figure 2***.

2.5 EDLC Fabrication

Planetary ball miller (XQM-0.4) was employed to mix the 0.25 g of carbon black and 3.25 g of activated carbon (AC) at 500 rpm for around 20 minutes. Six metal balls were incorporated to a chamber together with the above powders. Then, 0.5 g of polyvinylidene fluoride (PVdF) was inserted in the solvent of 15 mL N-methyl pyrrolidone (NMP) and then stirred for 60 minutes. The powders were transferred into the PVdF-NMP solution and then stirred for 2 hours till the emergence of homogenous solution of dense black. An aluminum foil was cleaned using acetone and finally the synthesized homogenous solution was coated on it by using a doctor blade. Subsequently, the gained AC electrodes were dried-out in an oven at 60 ˚C with the mass loading of active material of 2.43 mg. Finally, the dried AC electrodes were kept in a dessicator with silica gel for drying better. The formed electrodes were cut into circles with area of 2.01 cm^2. The mass of electrode minus with the mass of aluminum foil was 2.99 mg. From the mass mentioned earlier, AC was 81.25% from the total mass of each circle electrode. Hence, the mass of AC was 2.43 mg and was to calculate EDLC parameters because AC is the active mass.

2.6 EDLC Characterization

The AC electrodes were cut into circles with area of 2.01 cm^2. The utmost conducting PE (PGNC-4) was set in between two AC electrodes and laid in a CR2032 coin cell. Finally, the coin cell was located in a Teflon case as exhibited in ***Figure 3***.

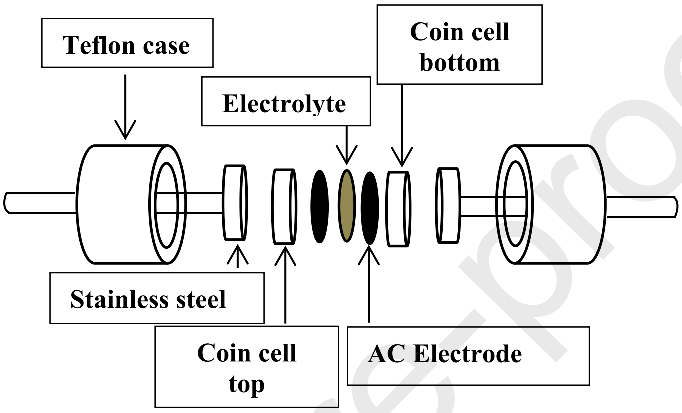

Figure 3. Design of the synthesized EDLC.

The cyclic voltammetry (CV) of the EDLC was taken with Digi-IVY DY2300 potentiostat. The applied potential was in the range between 0 V and 0.9 V with various scan rates. The EDLC displayed in ***Figure 3*** was exposed with several scan rates of 5, 10, 20, 50, and 100 mV s^{-1}. The specific capacitance C_{CV} of the EDLC at the several scan rates can be developed from the CV profile through the following relation [32]:

$$C_{CV} = \int_{V_i}^{V_f} \frac{I(V)dV}{2mv(V_f - V_i)} \qquad (3)$$

The CV plot area ($\int I(V)dV$) can be acquired using function of integration in Origin 9.0 software. v refers the scan rate, m refers the mass of activated carbon (2.43 mg), V_f and V_i are the final voltage of 0.9 V and the initial voltage of 0 V, respectively. The

EDLC rechargeability is checked via NEWARE battery cycler for 1000 cycles at a current density of 0.5 mA cm^{-2} or 0.33 mAg^{-1}. The surroundings for analysis the CV and EDLC charge-discharge was settled at ~25 ˚C and relative humidity of ~50%. The specific capacitance (C_d) using discharge curve can be found from Eq.(4) [32]:

$$C_d = \frac{i}{xm} \tag{4}$$

Here i and x denote applied current and gradient of discharge part, respectively. The C_{CV} and C_d values of the EDLC were compared so as to check the confidence of the results. The situation of the contact between the electrode and CPE of the EDLC device was validated by means of the following equation [32]:

$$ESR = \frac{V_d}{i} \tag{5}$$

Where ESR denotes equivalent series resistance and V_d denotes potential drop before discharging process.

3 Results and discussion

3.1 XRD Examination

The XRD pattern of pure PVA and PVA:NH_4SCN:Cu(II)-complex:GLY are displayed in ***Figure 4***. A couple of peaks at nearly 2θ = 20° and 40° in the XRD spectrum of pure PVA are noted, which have been related to the crystalline structure of PVA in previous investigations [33, 34]. It is clear that these peaks still exist in the XRD spectra of PVA:NH_4SCN:Cu(II)-complex:GLY even though their intensities were considerably decreased. More explicitly, the peak at 2θ = 40° almost disappeared, whereas the peak at 2θ = 20° widened. The extension of the amorphous nature is ascribed in the wideness increase and fall in the peak intensity at $2\theta = 20^{\circ}$ [35, 36].

The doping of salt to the host polymer is probable to raise the structure of amorphous nature in PE. In an earlier research, the XRD pattern of starch-chitosan:NH_4Cl SPE system showed a clear increase in the crystalline peaks with emerging additional crystalline peaks at maximum salt concentration [28]. This outcome designated the salt recrystallization and ions recombination, which resulted in the decrement of free ions density, and therefore declined the σ_{DC} [28]. Different approaches were specified to overcome these challenges. One of the approaches is the addition of Cu(II)–complex to the PE in order to develop the amorphous structure and increase the σ_{DC}. The addition of GLY to the electrolyte was also attempted to further improve the σ_{DC}. The amorphous structure in the electrolyte complexes can be enhanced with the inclusion of GLY [37]. The existence of GLY in the complex systems helps salt dissociation, which in turn restricts salt recrystallization. Moreover, the plasticizer can produce different pathways for ions conduction; therefore, assisting the polymers to accommodate more salt. These processes raise the amorphous phase in the PEs, subsequently enhancing the electrolyte σ_{DC} [28]. The ion conduction is desirable in the amorphous structure owing to segmental movement of polymer chains [38, 39]. Moreover, the absence of any XRD peaks associated with pure PVA, approves the whole dissociation of NH_4SCN salt in the PE [38]. The elimination of hydrogen bonding among the polymer chains causes broadening and weakening in intensity, which signifies the dominance of the amorphous phase in the PE system [33].

The addition of GLY and Cu(II)–complex will result in the intensity reduction of crystalline peaks and vanishes the crystalline peak at $2\theta = 20^{\circ}$ (see ***Figure 4***). In our previous work, it was shown that when Cu(II)-complex was added to the PVA host polymer, the amorphous nature expanded, which was noted as a decrease in the intensity of the XRD spectra [29]. The Cu(II)-complex XRD pattern in our earlier work indicated that the prepared Cu(II)-complex is nearly amorphous, thus the crystalline peaks cannot be perceived through the whole range of 2θ degrees. Obviously, just a hump can be seen from $2\theta = 20^{\circ}$ to 30° [29]. The XRD analysis results approve that a good complexation took place between the PVA and the electrolyte components.

The deconvolution technique for the XRD spectra was used to determine the potential amorphous peaks and the crystalline peaks and it was also used to determine the degree of crystallinity (*Xc*) [39], as shown in ***Figure 4***. The large and wide peaks signify the amorphous peaks, while the narrow, sharp and small peaks indicate the crystalline peaks. Pure PVA possesses *Xc* of 41.68, which is noticeably decreased when GLY is inserted. Thus, the amorphous structure of the systems is enhanced with the GLY insertion. It is seen in ***Figure 4*** that when GLY is added, crystalline peaks in PGNC-1 became smaller and less sharp (***Figure 4 (c-e)***). The addition of GLY with 40 wt.% gives rise to the smaller crystalline peaks, as seen in the XRD pattern of PGNC-4 (***Figure 4(e)***). Eq. (6) was used to obtain *Xc* for pure PVA and doped PVA and the *Xc* values are tabulated in ***Table 1***. PGNC-1 system has *Xc* value of 8.93 while PGNC-4 has the minimum *Xc* value of 3.54, meaning that the PGNC-4 is the highest amorphous system in this study [39].

$$Xc = \frac{A_C}{A_T} \times 100\% \qquad (6)$$

Here, A_T and A_C refer the total area of the amorphous and crystalline peaks and total area of the crystalline peaks, respectively, which were accomplished by the deconvolution method using the OriginPro software. The Gaussian function mode was employed for the fitting of the XRD spectra.

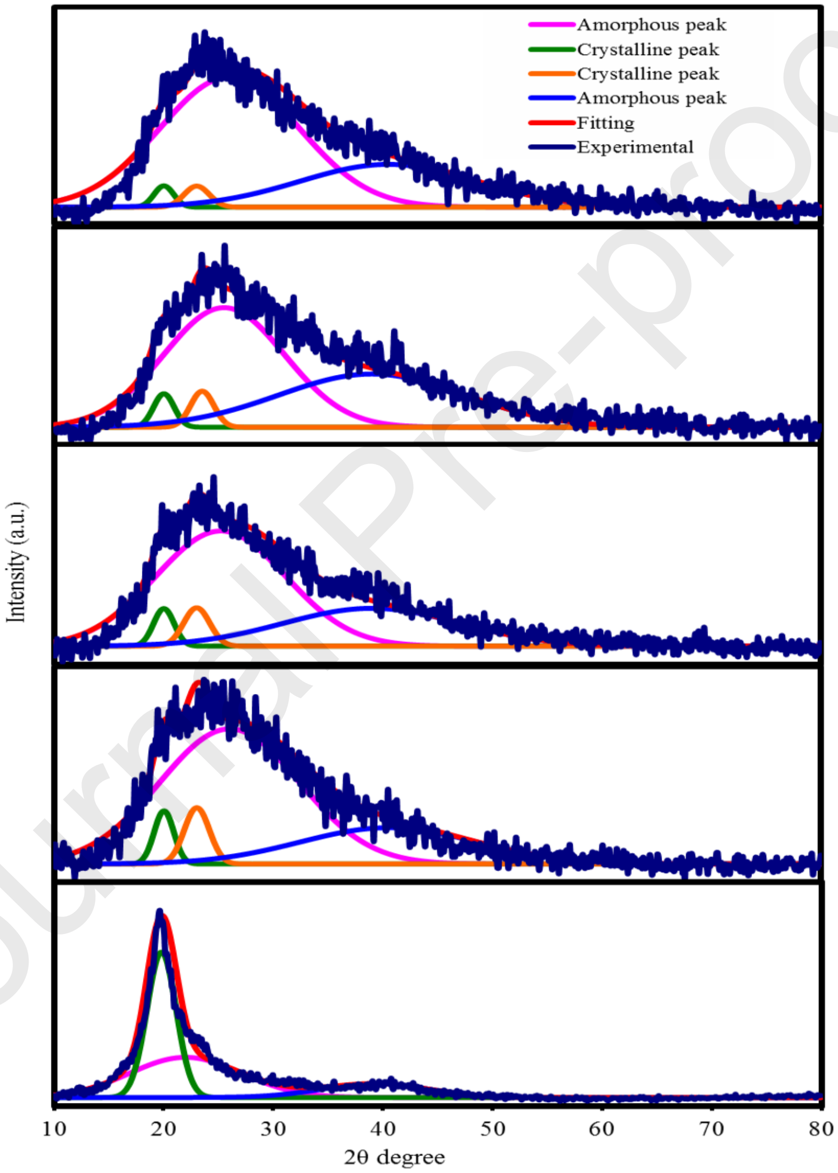

Figure 4. XRD spectra for (a) pure PVA, (b) PGNC-1, (c) PGNC-2, (d) PGNC-3, and (e) PGNC-4 films.

Table 1. The degree of crystallinity from deconvoluted XRD analysis

Electrolyte	Degree of crystallinity (%)
Pure PVA	41.68
PGNC-1	8.93
PGNC-2	7.54
PGNC-3	5.88
PGNC-4	3.54

3.2 FTIR Analysis

The FTIR spectra for pure PVA and PVA:NH_4SCN:Cu(II)-complex:GLY are shown in ***Figure 5***. The following modifications in the spectral features have been detected after comparing the spectra of pure and doped PVA. C–H rocking of pure PVA is considered the reason for absorption peak at 838 cm^{-1} (see ***Figure 5a,***) [33]. In the case of PVA:NH_4SCN:Cu(II)-complex:GLY, this peak shifted and its intensity decreased; whereas, upon the addition of 40 wt.% of GLY it nearly vanished.

It is well-known that in NH_4SCN salt–polymer, the charge carrier species are hydrogen ions (H^+) [24]. The new strong and intense peak detected at 2045 cm^{-1} is endorsed to aromatic S–C=N stretching of anion of SCN^- group of NH_4SCN. This band shifts with considerable intensity reduction upon the addition of the higher GLY concentration is related to the complexation with PVA functional groups (see ***Figure***

5b) [34, 38]. In the ammonium ion NH_4^+ tetrahedral, since just one of the four protons (H^+) weakly linked to the nitrogen atom; thus, the H^+ will transfer to every coordinating site of PVA. The change in peak place with the emergence of the new peak in the PVA:NH_4SCN:Cu(II)-complex:GLY indicates the complex creation amongst the PVA and the NH_4SCN [34]. The insertion of plasticizer helps further ions dissociation; therefore, additional ions are offered to create interactions with the functional groups of PVA [40]. Furthermore, the interaction between PVA functional groups and Cu(II)–complex was indicated in our previous work [29]. This interaction or the adsorption of Cu(II)–complex on the functional groups of the PVA is the two endorsed clarifications for the band intensity reduction [29]. Consequently, since adsorption causes an increase in the molecular weight, there is a reduction in the functional groups vibrational intensity [35].

In the meantime, O–H stretching vibration of hydroxyl (OH) groups can be related with the wide and robust absorption peak at 3340 cm^{-1} [41]. This band possesses a high intensity, almost certainly owing to the robust intra and inters kinds of hydrogen bonding [33]. Additionally, this band shifts and peak intensity drops in the PVA:NH_4SCN:Cu(II)-complex:GLY owing to its complexation with NH_4SCN salt and Cu(II)-complex. The peak at around 1643 cm^{-1} in the pure PVA is believed to be originated from the C=O stretching of acetate group [42], in which for the doped PVA films it is shifted to a smaller wavenumber. C–H asymmetric stretching vibration is related with a band at 2913 cm^{-1} [41], which also shifted and reduced considerably in the case of doped PVA films. Furthermore, the characteristic of –C–O– stretching vibration in pure PVA is ascribed through the peak at 1076 cm^{-1} [43], which is shifted with dropped intensity in the doped films with Cu(II)-complex and GLY, as shown in ***Figure 5a***.

The C–H bending vibration of CH_2 wagging has been recognized as the cause for the pure PVA absorption peak at 1419 cm^{-1}, while C–H deformation vibration has been related with the 1317 cm^{-1} absorption peak in pure PVA (see ***Figure 5a,***) [42]. It is therefore clear that the PVA:NH_4SCN:Cu(II)-complex:GLY samples were related with shifting of these two peaks and a considerable reduction in the intensity of these peaks. These modifications in the FTIR spectra are strong evidences for the interaction of PVA functional groups with the electrolyte components (see ***Figure 5a, b***).

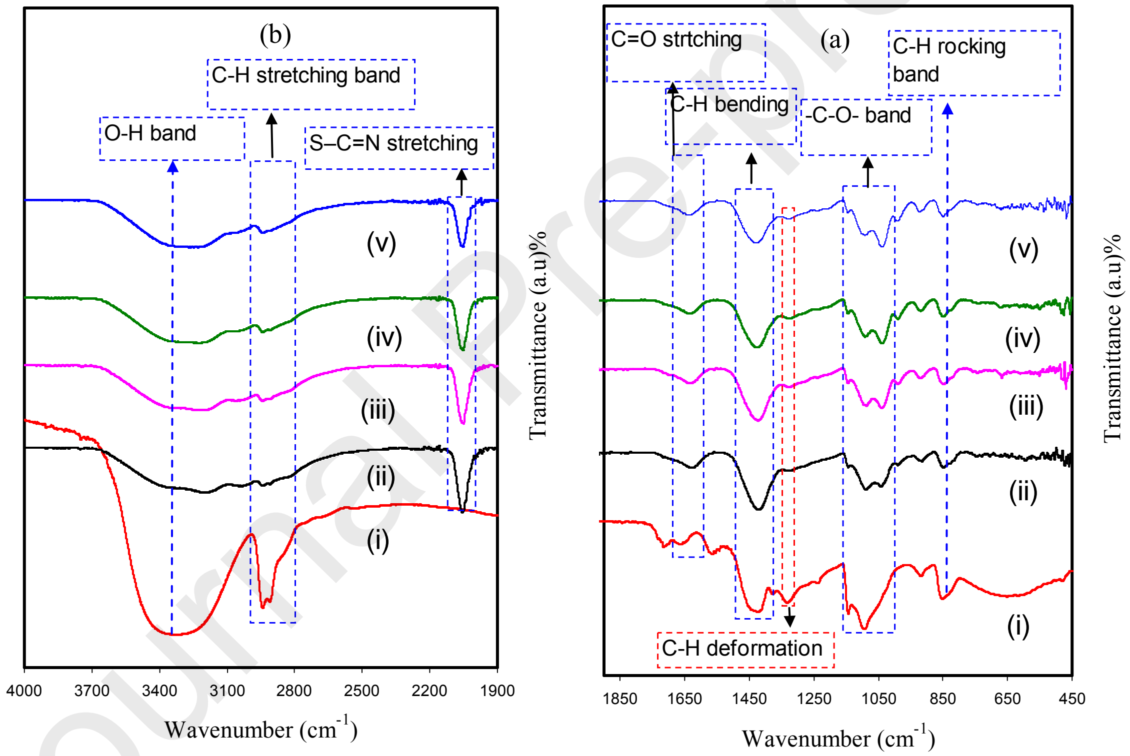

Figure 5. Spectra of FTIR for (i) pure PVA, (ii) PGNC-1, (iii) PGNC-2, (iv) PGNC-3, and (v) PGNC-4 in the range (a) 450 cm^{-1} to 1900 cm^{-1}, and (b) 1900 cm^{-1} to 4000 cm^{-1}.

3.3 Morphological Study

Figure 6a(i-iv) illustrates surface morphology of all the studied films through FESEM images. It is recognized that the surface morphology of the PE films is the key properties to recognize their behavior [44]. The images were obtained at 500× magnification. The small grey lumps can be seen on the surface of the CPE films (see ***Figure 6a(i)***). These lumps were attributed to the protrude salts. It is evident from the images that the grey lumps are disappeared as the GLY concentration was increased from 20 to 40 wt.%. The CPE has a smooth and uniform surface morphology without existing a phase separation as shown in ***Figure 6a(ii-iv)***. It is well documented that smooth morphology appearance is related to the amorphous phase of the PE system [45]. The smooth surface electrolytes can assist conducting ionic species to pass more easily, and therefore increases the value of σ_{DC} [45]. Likewise, the CPE samples with uniform surface in ***Figure 6a(ii-iv)*** indicates the fine dispersion of Cu(II)-complex. The small white spots appearing on the CPE films surface are attributed to Cu(II)-complex.

This was though, certified to be different in previous works, while extra agglomerated particles on the surface of the CPE films appeared as excessive fillers was included in the polymers. For examples, Hamsan et al. [46] determined the σ_{DC} decrement as more GLY was inserted. It has been explained that this is ascribed to the rearrangement of self-linkages of plasticizer producing recrystallization of salt which causes a decrease in σ_{DC} [47]. Hence, polymer capability is restricted to accommodate extra salts, which in turn caused recrystallization of salt [48]. Lim et al. [1] have also connected the surface morphology of CPEs to the σ_{DC}. In their work, a fall in σ_{DC} upon addition of 10 wt.% TiO_2 has been shown for PVA:$LiClO_4$:TiO_2 electrolyte systems. They proposed that this observation is due to the agglomeration of TiO_2. They related this to the fact that, the CPE surface morphology possesses great level of rigidity owing to the addition of 10 wt.% TiO_2. Thus, these agglomerations could block conducting pathways for ionic movements. Large rigidity in the back bone of polymer also decreases the ion mobility. Consequently, the σ_{DC} is reduced with the blocking impact and ion transportation is limited.

It is believed that so as to accomplish high σ_{DC}, the surface has to be smooth uniform. In other words, it is linked to the film amorphous structure [49]. The addition of Cu(II)-complex improved the amorphous phase further as shown in our previous work [29]. In fact, the interaction between the PVA and electrolyte's components is evinced by the smooth uniform surface morphology of the CPE samples (see ***Figure 6a(i-iv)***).

In this study, the outcomes display that there is an innovation of the PE preparation as a novel and simple technique to get a great σ_{DC} and high performing EDLC. The FESEM images are in good agreement with the XRD and FTIR results. From the XRD and FTIR routes, the interaction among the PVA and electrolyte's components were validated. It is indicated that the CPE surface morphology is observed to be nearly smooth and uniform without having obvious protruded salts at high GLY concentration. From these outcomes, the fabricated CPE was well-defined with amorphous behavior even at the maximum GLY amount. The role of GYL content on increasing free ionic species in the prepared samples is schematically illustrated in ***Figure 6b***.

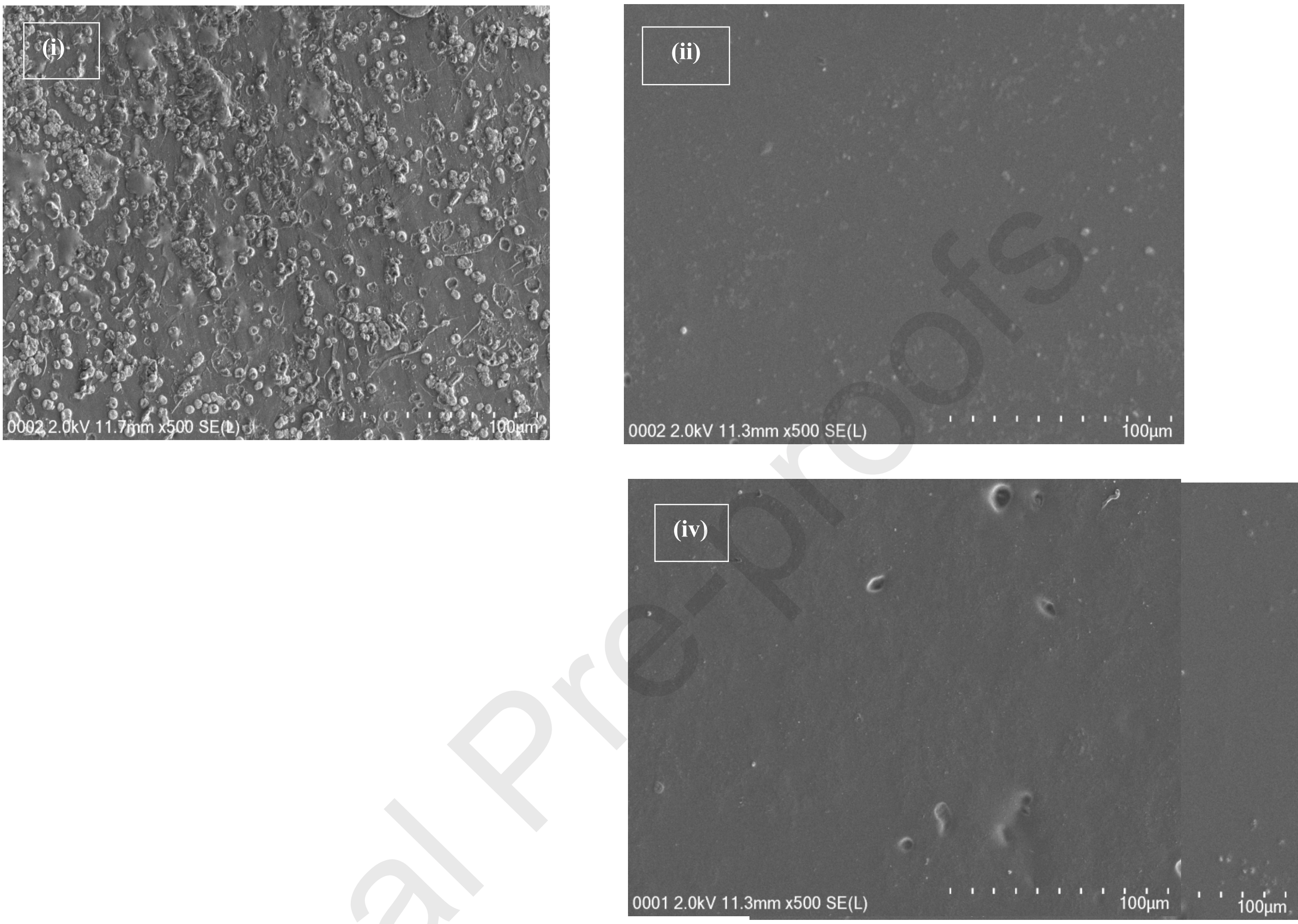

(a)

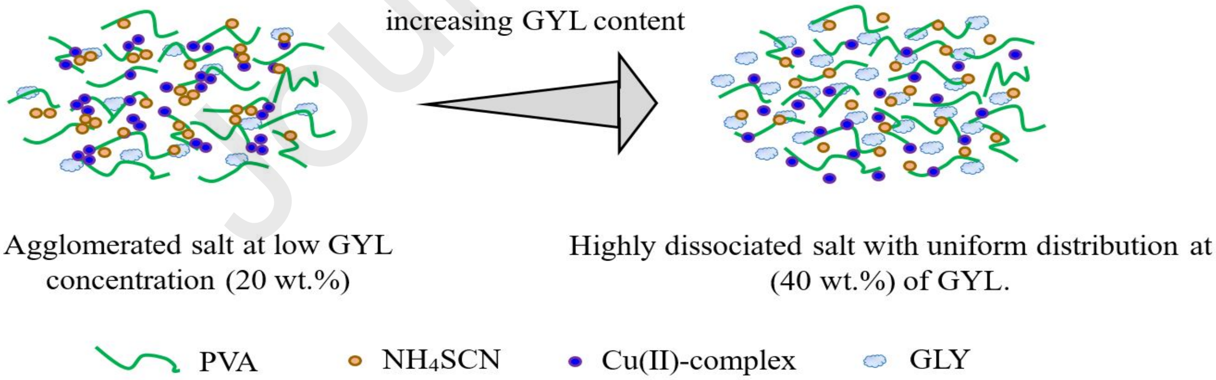

Figure 6. (a) Field emission scanning electron microscopy (FESEM) for (i) PGNC-1, (ii) PGNC-2, (iii) PGNC-3, and (iv) PGNC-4 electrolytes. (b) Schematic illustration of the role of GYL content on ion dissociation.

(b)

3.5 Impedance Analysis

The electrochemical and ion transference behaviors of ionic materials, for example electrodes and PEs, can be efficiently examined by the use of electrochemical impedance spectroscopy (EIS) [50, 51]. In this work, EIS was used to analyze the impedance plots for the CPE films (see ***Figure 7(a-d)***). For PGNC-1 system in ***Figure 7a***, a semicircle at high frequency region is resulted from the CPEs bulk effect, and a tail at low frequencies can be noted. The tail at the low frequencies happens because of the creation of the EDLC through the free charges buildup at the electrode and electrolyte interface [52]. The spike or tail was only displayed by the other samples (see ***Figure 7(b-d)***).

The electrical equivalent circuit (EEC) method is used as a straightforward way for the EIS examination, which provides the entire image of electrolyte system [53]. The Nyquist plot for the systems was deduced in terms of the EEC. It comprises bulk resistance (R_b) for the carriers in the electrolyte systems and two constant phase elements (CPE) as seen in the insert of ***Figure** 7*. The region of high frequencies displays the connection of R_b and constant phase element in parallel, while the region of low frequencies indicates only constant phase element, meaning that the formed EDLC between electrode and electrolyte. The constant phase elements term is more usually employed in EEC rather than ideal capacitor in the real system.

The impedance of Z_{CPE} can be written as [46,54]:

$$Z_{CPE} = \frac{1}{C\omega^{p}}\left[\cos\left(\frac{\pi p}{2}\right) - i\sin\left(\frac{\pi p}{2}\right)\right] \tag{7}$$

Where C stands for the constant phase element capacitance, ω refers the angular frequency and p is linked to the departure of the EIS plots from the vertical axis. Here, the real (Z_r) and imaginary (Z_i) parts of complex impedance (Z^*) correlated with the EEC (insert of ***Figure 7a***) are indicated as [54]:

$$Z_r = R_s + \frac{R_b C_1 \omega^{p1} \cos\left(\frac{\pi p_1}{2}\right) + R_b}{2R_b C_1 \omega^{p1} \cos\left(\frac{\pi p_1}{2}\right) + R_b{}^2 C_1{}^2 \omega^{2p1} + 1} + \frac{\cos\left(\frac{\pi p_2}{2}\right)}{C_2 \omega^{p2}} \tag{8}$$

$$Z_i = \frac{R_b C_1 \omega^{p1} \sin\left(\frac{\pi p_1}{2}\right)}{2R_b C_1 \omega^{p1} \cos\left(\frac{\pi p_1}{2}\right) + R_b{}^2 C_1{}^2 \omega^{2P1} + 1} + \frac{\sin\left(\frac{\pi p_2}{2}\right)}{C_2 \omega^{p2}} \tag{9}$$

Where C_1 refers the bulk constant phase element capacitance and C_2 refers the constant phase element capacitance at the interface of electrode and electrolyte.

Here, the Z_r and Z_i parts of Z^* associated with the EEC (inset of ***Figure 7b-d***) are expressed as [54]:

$$Z_r = R_s + \frac{\cos\left(\frac{\pi p_2}{2}\right)}{C_2 \omega^{p2}} \tag{10}$$

$$Z_i = \frac{\sin\left(\frac{\pi p_2}{2}\right)}{C_2 \omega^{p2}} \tag{11}$$

Table 2 outlines the fitting parameters of the EEC. The R_b is obtained by the interception between the real axis and the spike. It is obvious that upon the addition of the GLY, the semicircle at the region of high frequencies were absent (see ***Figure 7b-d***) due to the complete transport of ions toward the electrodes. The R_b is dropped as the GLY amount increases to 40 wt% because of the increase in mobility of charge species, ensuring the rise in the σ_{DC} of ions. The increase in σ_{DC} with the GLY amount is consistent with the FESEM results (see ***Figure 6***). The addition of Cu(II)–complex to the PE significantly promoted the amorphous nature that caused to increase the σ_{DC} and improve the EDLC performing. Rangasamy et al., [55] thought that the increase in the amorphous phase of the PE increases the ions mobility by developing more free volume in the PE system. This leads to an increase in the polymer chains segmental motion, due to the rise in the polymer chains flexibility. Therefore, the σ_{DC} in the PE can be improved. Liew [56] had developed the CPE based on PAA:LiTFSI with the insertion of $BaTiO_3$. The author obtained σ_{DC} of 5×10^{-4} S cm^{-1} and used the CPE in the EDLC cells. This indicates that CPE is a good candidate to be employed as a PE in the EDLC device. By considering the R_b value and the CPE dimensions, the σ_{DC} of the CPE films can be calculated using the relation below [57],

$$\sigma_{dc} = \left(\frac{1}{R_b}\right) \times \left(\frac{t}{A}\right) \tag{12}$$

Where t denotes the CPE thickness. A refers to the area of the SS electrode. The values of σ_{DC} of the CPE samples are listed in ***Table 3***. Previous reports have indicated that PEs with high σ_{DC} in the range between 10^{-5}- 10^{-3} S cm^{-1} can be employed for use in EDLCs (see ***Table 4***). The σ_{DC} value of the synthesized EDLC is in comparison with previous works using a number of PEs as recorded in ***Table 4***. The idea of σ_{DC} value was supported in the sense that the σ_{DC} depends on the charge number density (n_i) as well as ionic mobility (μ_i), as follows [58],

$$\sigma_{dc} = \sum_i n_i q_i \mu_i \tag{13}$$

Here q_i stands for the charge of the species (1.6×10^{-19} C). There was an increase in σ_{DC} when n_i and μ_i inside the system of PE increases, as it is apparent from Eq. (13). The ***Table 3*** data as well as EIS spectra in ***Figure 7*** obviously indicate that having more GLY concentration will give rise to the value of σ_{DC}. GLY decreases the attraction force between the cations and anions of the salt [27, 28]. Thus, a greater number of ammonium ions (n_i) is offered by NH_4SCN to the polymer.

Table 2. The fitting parameters of the EEC for CPEs system at room temperature.

Sample	P_1 (rad)	P_2 (rad)	K_1 (F^{-1})	K_2 (F^{-1})	C_1 (F)	C_2 (F)
PGNC-1	0.814768	0.383195	1.20×10^{9}	9.20×10^{4}	8.33×10^{-10}	1.09×10^{-5}
PGNC-2	-	0.668364	-	8.60×10^{4}	-	1.16×10^{-5}
PGNC-3	-	0.706885	-	3.20×10^{4}	-	3.13×10^{-5}
PGNC-3	-	0.681095	-	2.27×10^{4}	-	4.41×10^{-5}

Table 3. Achieved σ_{DC} of the PVA:NH_4SCN:Cu(II)-complex:GLY system at room temperature.

Designation	Composition (PVA wt.%:NH_4SCN wt.%:Cu(II)–complex mL:GLY wt.%:)	R_b (Ohm)	σ_{DC} (S cm^{-1})
PGNC-1	50:50:10:10	2.28×10^4	5.23×10^{-7}
PGNC-2	50:50:10:20	50	3.24×10^{-4}
PGNC-3	50:50:10:30	12	1.46×10^{-3}
PGNC-4	50:50:10:40	11	2.25×10^{-3}

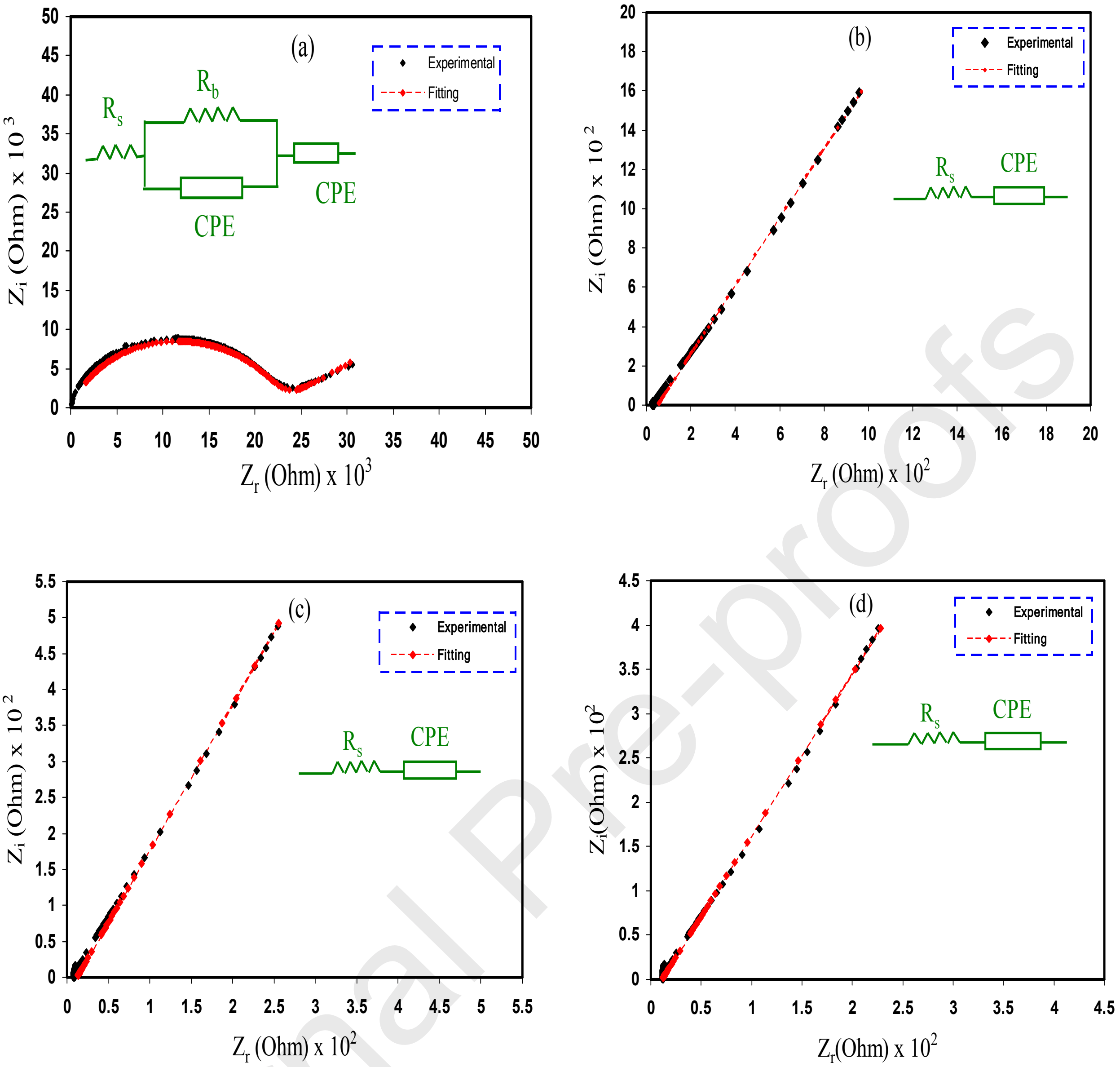

Figure 7. Experimental EIS for (a) PGNC-1, (b) PGNC-2, (c) PGNC-3, and (d) PGNC-4 electrolyte films.

Table 4. DC conductivity (σ_{DC}) specific capacitance (C_d), energy density (E_d), power density (P_d), and cycle number of EDLCs using dissimilar PEs at room temperature.

Electrolyte composition	σ_{DC} (S cm^{-1})	C_d (F g^{-1})	E_d (Wh kg^{-1})	P_d (W kg^{-1})	Cycle No.	Ref.
PVA:$LiClO_4$:TiO_2	1.3×10^{-4}	12.5	1.56	198.7	1000	[1]
CMC:KC:NH_4NO_3	$\sim10^{-4}$	20	-	-	10000	[59]
Chitosan:H_3PO_4:NH_4NO_3:Al_2SiO_5	$(1.82 \pm 0.1) \times 10^{-4}$	0.2	-	-	100	[60]
PAA:LiTFS:$BaTiO_3$	5×10^{-4}	34.22	3.32	71.47	20000	[56]
PDMA: $MgTf_2$: Co_3O_4	9.4×10^{-3}	29.48	1.89-2.62	157.7-240.4	8000	[19]
Dextran:NH_4Br	$(1.67 \pm 0.36) \times 10^{-6}$	2.05	-	-	100	[61]
PS:MC:NH_4NO_3:GLY	$\sim10^{-3}$	31	3.1	910-385	1000	[46]
PVA:chitosan:NH_4NO_3:EC	1.6×10^{-3}	27.1	-	-	100	[62]
MC:NH_4Br:GLY	$(1.89 \pm 0.05) \times 10^{-4}$	-	-	-	-	[49]
Chitosan:MC:NH_4I	6.65×10^{-4}	9.97	1.1	578.55	100	[14]
PVA:Naft:BmImBr	2.31×10^{-3}	16.32	-	-	1000	[17]
Chitosan:MC:NH_4F	2.96×10^{-3}	58.3	7.3	964	100	[18]
PVA:CH_3COONH_4:BmImBr	$(9.29 \pm 0.01) \times 10^{-3}$	21.89	1.36	34.66	500	[63]
PVA:dextran:NH_4I	2.08×10^{-5}	4.2	0.55	64	100	[64]
MC:NH_4NO_3:PEG		38	3.9	140	100	[65]
MC:dextran:NH_4I	1.12×10^{-3}	79	8.81	1111.1–170	100	[66]
Cellulose acetate:$LiClO_4$	4.9×10^{-3}	90	-	-	600	[67]
EMIM-TFSI:PVDF-HFP	-	51.8	15.7	1048	3000	[68]
PVA:NH_4SCN:Cu-complex:Gly	2.25×10^{-3}	155.32	17.473	4960	1000	This work

Where; $LiClO_4$ = Lithium perchlorate, TiO_2 = Titanium dioxide, CMC = Carboxymethyl cellulose, KC = kappa carrageenan, NH_4NO_3 = Ammonium nitrate, Al_2SiO_5 = Aluminium silicate, PAA = Poly(acrylic acid), LiTFS = lithium bis(trifluoromethanesulfonyl)imide, $BaTiO_3$ = barium titanate, PS = Potato starch, MC = methylcellulose, EC = ethylene carbonate, CH_3COONH_4 = Ammonium acetate, BmImBr = 1-butyl-3-methylimidazolium bromide, PEG = poly (ethylene glycol), EMI-TFSI= 1-ethyl-3-methylimidazolium bis(trifluoromethanesulfoly) amide, PVdF= poly(vinylidene fluoride), HFP= hexafluoropropylene, PDMA= poly (N, N-dimethylacrylamide), $MgTf_2$= Magnesium trifluoromethanesulfonate, Co_3O_4= Cobalt oxide, Naft= sodium trifluoromethanesulfonate, BmImBr= 1-butyl-3-methylimidazolium bromide, NH_4F= Ammonium fluoride.

3.6 EDLC Characteristics

3.6.1 Transference Number Measurement (TNM)

TNM is employed to identify the highest carrier species inside the CPE. When 0.2 V is applied, the current commences to decrease until it gets saturation. The current polarization set against time for the maximum conducting CPE (PGNC-4) is portrayed in ***Figure 8***. The cause for the enormous of the early current value is in consequence of the part held by the ion and the electron carriers at the early stage. ***Figure 8*** illustrates that there is a substantial reduction in the current prior it reached an equilibrium state. Once the CPE was polarized, it is in the equilibrium; whereas, the maintained current movement is owing to electron species. The cause for that is the blocking of ions caused by the SS electrodes, which lets only the electron to transport through it [69]. Eqs. (1) and (2) are employed to evaluate t_{ion} and t_{el} values, which obtaining I_i and I_{ss} values as 279.9 μA and 8.1μA, respectively. The t_{ion} and t_{el} values are established to be 0.971 and 0.029, respectively. It is interesting to note that the t_{ion} is very close to the ideal value of one. Subsequently, it is concluded that ions have a significant role in the transportation mechanism in the PVA:NH_4SCN:Cu(II)–complex:GLY system.

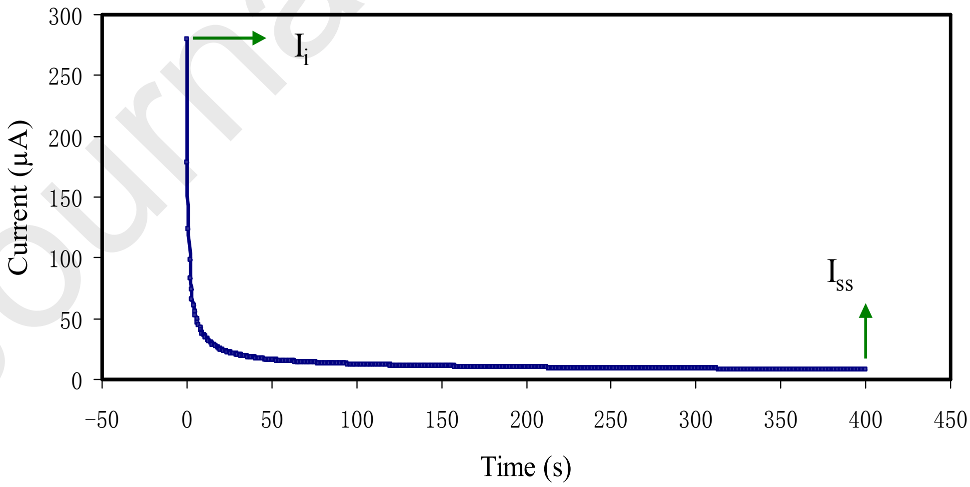

Figure 8. Polarization current versus time for the maximum conducting (PGNC-4) CPE film.

3.6.2 Electrochemical Stability Study

The electrochemical stability window (ESW) is an essential characteristic to be studied [70]. Hence, linear sweep voltammetry (LSV) measurement is led to find the PE decomposition voltage. The device performance is verified when one is alert of the ESW of the PE film prior the test of charge-discharge cycles. To avoid causing any harm to the PE, the decomposition voltage is vital. ***Figure 9*** depicts the LSV plot of PGNC-4 at 10 mV s^{-1} with a voltage range of 0 to 2.5 V. There is no obvious change in the current within the working electrode in the voltage varying from 0 to 2.15 V. ESW is observed at 2.15 V as the current starts to raise drastically, revealing CPE decomposition.

This outcome is similar to the work by Liew [56] on PAA:LiTFSI:$BaTiO_3$ CPE with ESW of 2.3 V. They employed the CPE in an EDLC. Kadir & Arof [62] reported that the ESW for PVA-chitosan-NH_4NO_3-EC film is 1.70 V, which is lesser than the obtained result in our work. The usual ESW for protonic battery use is approximately 1 V [71]. Therefore, the decomposition voltage of PGNC-4 highlights its suitability for applications in protonic devices. Lim et al. [1] documented that the decomposition voltage of PVA:$LiClO_4$:TiO_2 was found to be 2.4 V and they used the CPE in an EDLC.

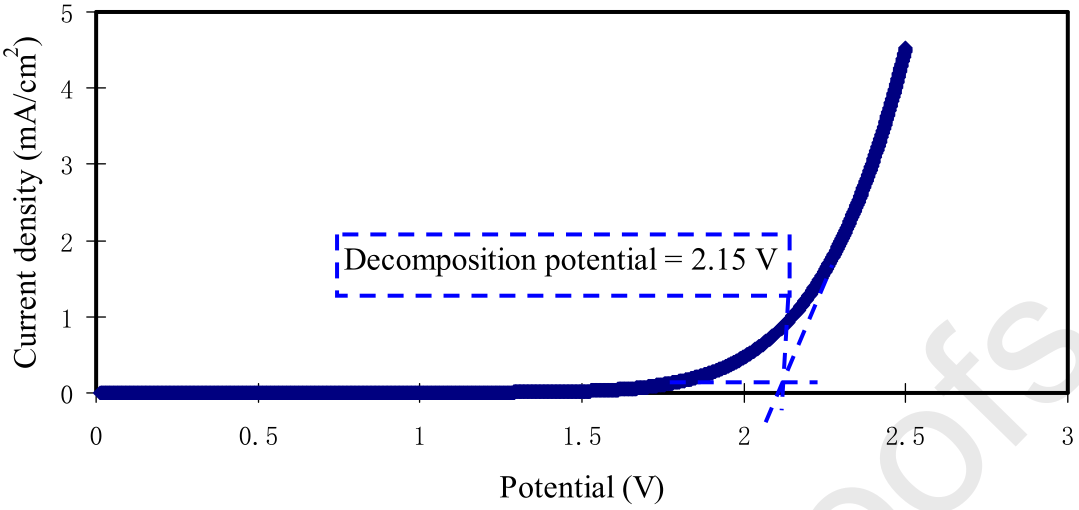

Figure 9. LSV plot for the maximum conducting (PGNC-4) CPE film.

3.6.3 Cyclic Voltammetry Study

Cyclic Voltammetry (CV) examination was employed to assess the performance of EDLC using PGNC-4 CPE. ***Figure 10*** shows the CV plot of EDLC at various scan rates of 5, 10, 20, 50, and 100 mV s^{-1}. No peak is seen in the CV plot signifying that no redox reaction happens at the potential range of 0 to 0.9 V. This is verified the existence of EDLCs [72]. As seen in ***Figure10***, the CV plot shape deviated from a leaf shape to a nearby shape of a rectangle when the scan rate decreases. High scan rate causes a departure of the CV plot from rectangular shape that is ascribed to the internal resistance and carbon porosity; hence, generating a current-voltage dependence [62]. The values of C_{CV} will be derived from the profile of CV with Eq. (3) and are presented in ***Table 5*** at different scan rates of 5, 10, 20, 50, and 100 mV s^{-1}. The value of C_{CV} increases as the scan rate drops. Ions use the whole vacant sites through the electrodes where ions have appropriate time for the mechanism of diffusion at short scan rates, causing in grander value of C_{CV} [73]. The CV shapes acquired in this work is similar to that achieved by Lim et al. [1]. In their study, the CV at the scan rates of 10, 30, 50, and 100 mV s^{-1} were created for EDLCs with the system of PVA:$LiClO_4$:TiO_2-based CPE.

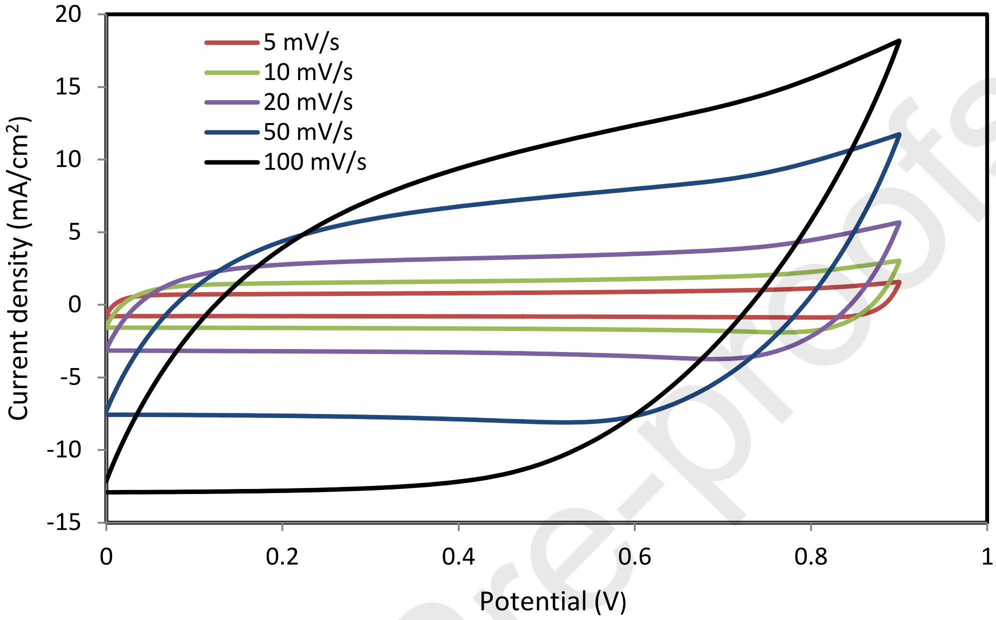

Figure 10. Cyclic voltammetry (CV) plot of the synthesized EDLC for the largest conducting (PGNC-4) CPE film.

Table 5. Capacitance values from CV as opposed to scan rates.

Scan rates (mv/s)	Capacitance (F/g)
100	64.014
50	100.137
20	123.457
10	132.602
5	134.889

3.7 Galvanostatic charge-discharge analyses

Figure 11a displays the EDLC charge-discharge profile at initial cycles at 0.5 mA cm^{-2} current density. The roughly discharge curves with linear slope designates the

EDLC capacitive manners [73]. The charge-discharge plot of the EDLC at 0.5 mA cm^{-2} for the selected cycles up to 1000th cycles is exposed in ***Figure 11b*, c**. It could be seen that the discharge slope is still almost linear, signifying the presence of capacitive behavior of the EDLC [73]. ***Figure 11b,c*** displays the charge-discharge performance of the EDLC at specific cycles. At the beginning of charge-discharge process more ions are available to form double layer thus providing longer discharge time. As the cycle number increase, the discharge time become shorter, this is due to recombination of ion to form ion pairs or triplets. The development of ion pairs reduces the charge double-layer.

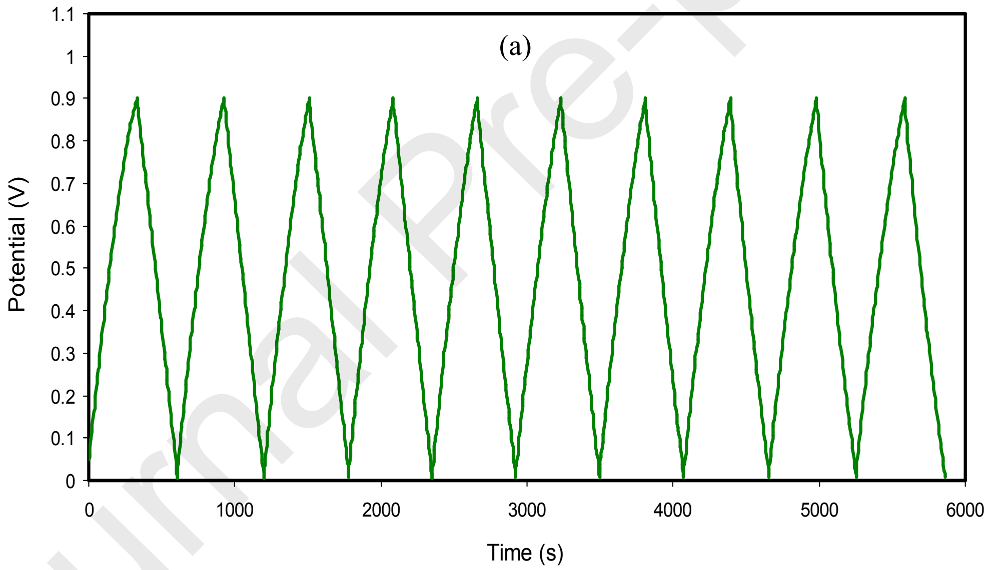

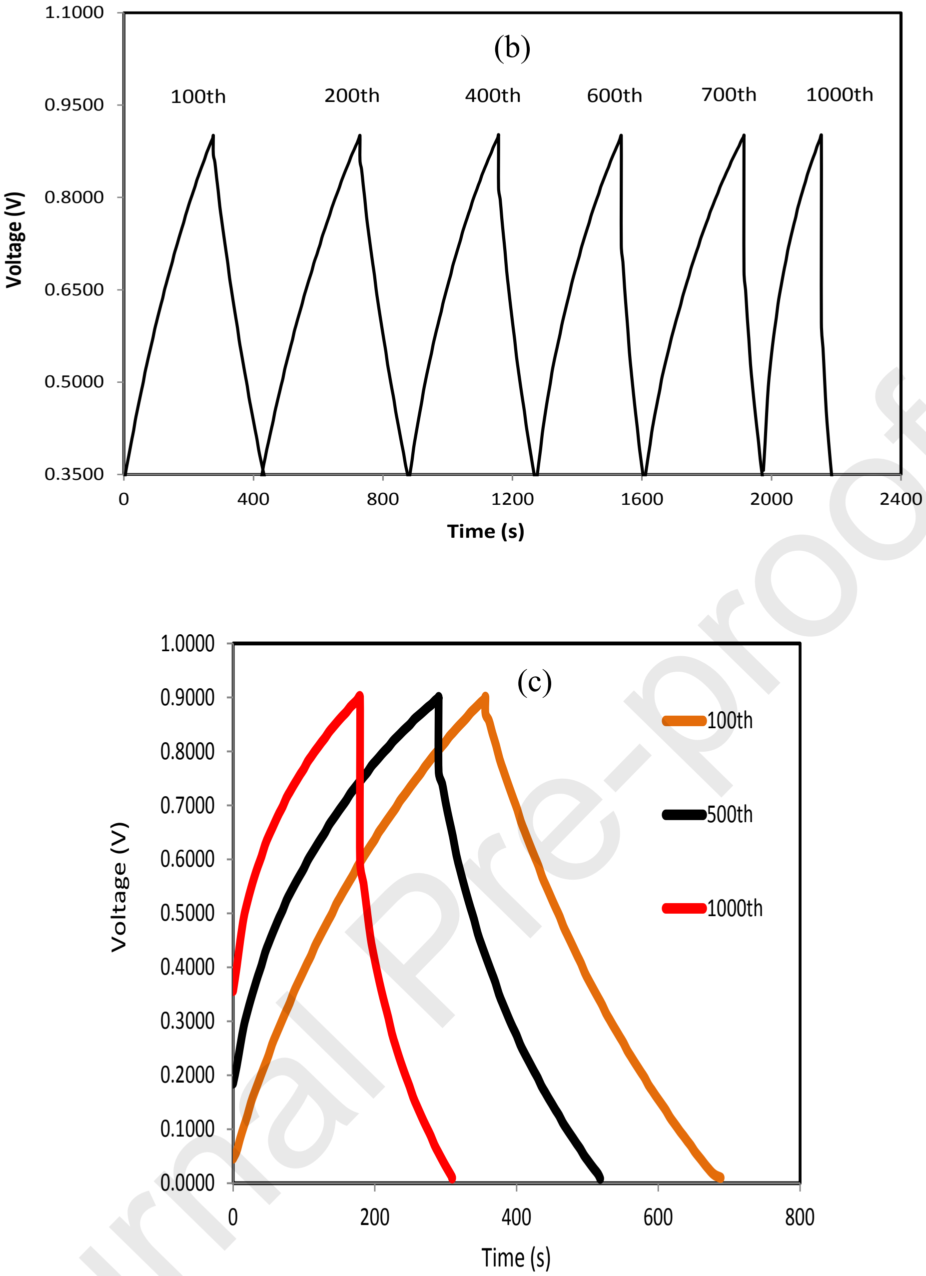

Figure 11. Charge–discharge profiles for the synthesized EDLC at 0.5 mA cm^{-2} for (a) initial cycles, (b) selected cycles of 100th, 200th, 400th, 600th, 700th, and 1000th and (c) selected cycles of 100th, 500th, and 1000th.

The value of C_d is computed by substitution the value of the slope of the discharge curves in Eq. (4). ***Figure 12*** displays the C_d versus number of cycles. The C_d value calculated for the 1st cycle is 128.6 F g^{-1}. This value is analogous to the C_{CV} obtained from CV examination (see ***Table 5***). Therefore, the C_d value accomplished from the EDLC in this study is responsible. The value of C_d was found to increase and stays constant with the average of 155.32 F g^{-1} besides the 1st cycle till it finishes 1000 cycles. Though, in previous documents significant decrease of C_d has been discerned with raising the number of cycles [1, 56]. The achieved C_d in this study is much higher than those stated in the literature using various PEs (see ***Table 4***).

The development of C_d in the EDLC is ascribed to the higher σ_{DC} value of the CPE due to the influence of the Cu(II)-complex on the enhancement of the amorphous structure [29], and the addition of GLY plasticizer [46]. As reported by Fan et al. [74], the development of the amorphous phase is to be beneficial in local chain segmental motion that can encourage the ions transportation and hence increasing the σ_{DC}. Thus, ions can transfer freely through the PE. Fast ion migration in the CPE also encourages the adsorption of ions at the interfaces of the electrodes and electrolytes that causes greater C_d value of EDLC [56].

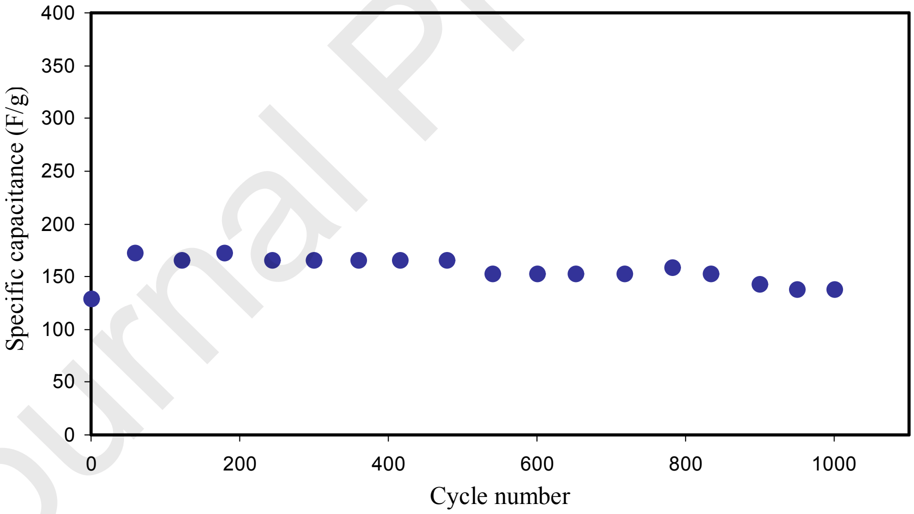

Figure 12. C_d of the synthesized EDLC for 1000 cycles.

The decrease in the voltage throughout the discharging process is caused by the EDLC internal resistance. The low drop voltage value, V_d, in this study denotes that less energy is dissipated during the charge-discharge process. The value of V_d is found by using Eq. (5) and displayed in ***Figure 13***. It can be seen that the increase in the value of V_d is still small throughout 1000 cycles, revealing the high performance of the fabricated EDLC. The EDLC internal resistance is attributed as equivalent series resistance (ESR). Therefore, a low ESR is crucial for the EDLC application. As documented by Arof et al. [75], the ESR in the EDLC is originated from the resistance of the current collectors, PE, and the space amongst the PE and the current collector. ESR is determined via Eq. (5), and the values are illustrated in ***Figure 14***. A best contact among PEs and electrodes would be achieved because of low ESR, meaning that the migration of ions to the pores at the electrodes surface would be efficient [76]. Kumar & Bhat [77] documented that the increase in V_d among the cycles of charge-discharge, which creates the increase in ESR is caused by the PE degradation in the EDLC. Fortunately, the increase in the ESR of the EDLC in the current work is still small within 1000 cycles. The ESR in the current study is much lower than the ESR values documented for other EDLC devices [59, 64].

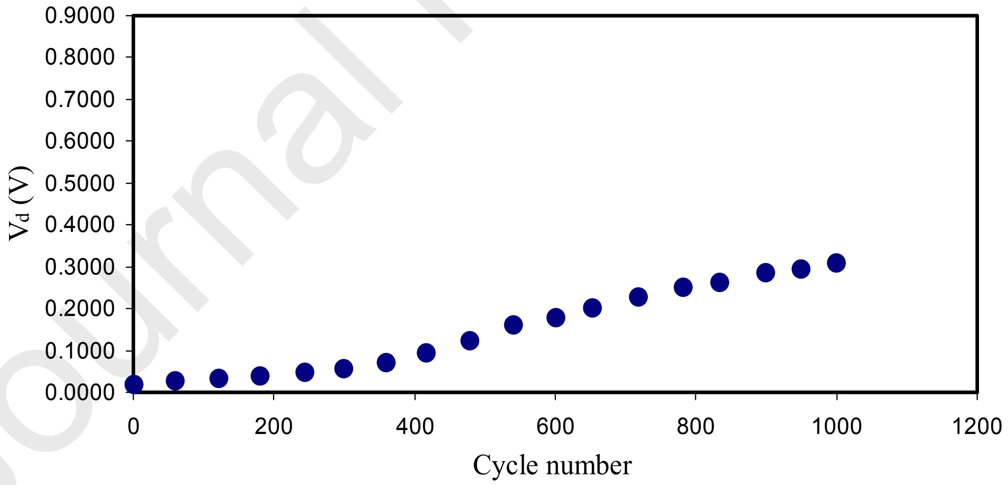

Figure 13. V_d **pattern of the fabricated EDLC for 1000 cycles.**

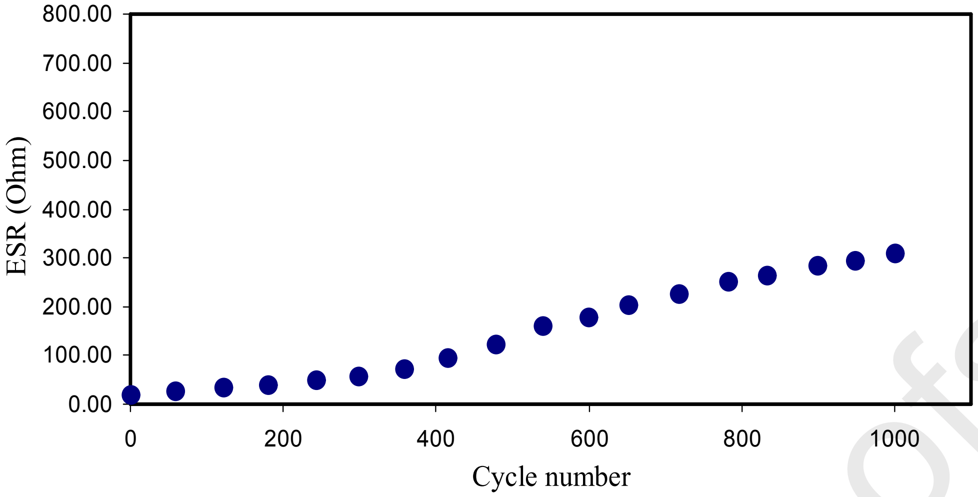

Figure 14. *ESR* pattern of the created EDLC for 1000 cycles.

The energy density (E_d) and power density (P_{d}) of the EDLC device are achieved using the following equations [14]:

$$E_d = \frac{C_s V}{2} \tag{14}$$

$$P_d = \frac{V^2}{4m(ESR)} \tag{15}$$

Where V denotes the used voltage.

From ***Figure 15***, it can be perceived that the value of E_d using Eq. (14) for the 1st cycle is 14.467 Wh kg^{-1}.The value of E_d exhibits an increase and continues constant with the average of 17.473 Wh kg^{-1} within the cycles beyond the 1st cycle up to 1000 cycles. It means that the same energy barrier is subjected by ions species in migration to the surface of the AC electrodes for the processes of charge-discharge within 1000 cycles. Though, in previous reports noticable decrease in E_d value were noted with increasing the cycle number [56, 63]. They described that the decrease in the value of E_d within the cycle number is ascribed to the raise in the ESR that creates the increase of energy loss through the mechanism of charge-discharge cycles [62, 78]. The accomplished E_d for the EDLC is sufficiently large compared to that described (3

Wh/kg) for PAA:LiTFSI:$BaTiO_3$- based CPE [56]. The obtained E_d in the current study is of the considerable attention in respect of the E_d value of roughly 1.56 Wh/kg that found for EDLC of the CPE system of PVA:LiClO4:TiO_2 [1]. Fortunately, the value of E_d (17.473 Wh kg^{-1}) within 1000 cycles in the current work is in the range of battery energy density and significantly higher than the E_d values reported in the literature (see ***Table 4***). These results indicate that the Cu(II)-complex as filler has a great impact on the performance of the EDLC device.

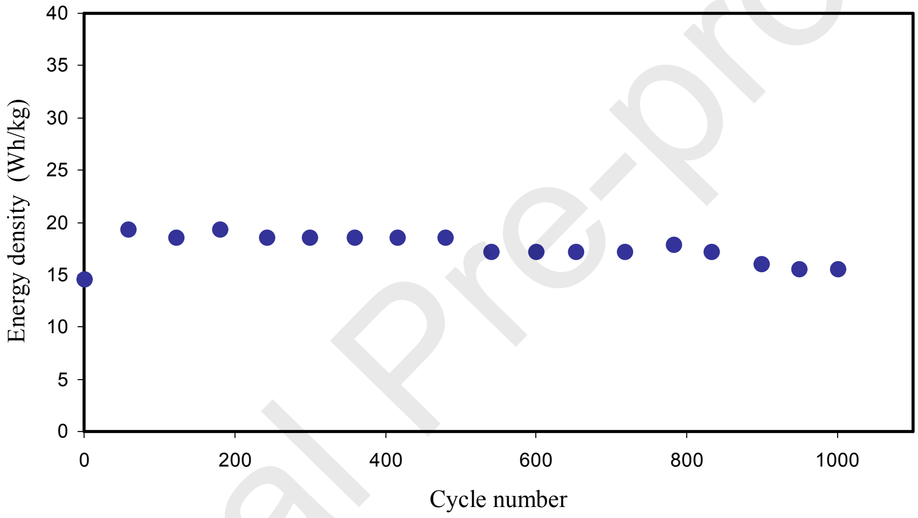

Figure 15. E_d of the synthesized EDLC for 1000 cycles.

The achieved P_d value using Eq. (15) for our study will be seen in ***Figure 16***. Over charge-discharge within 1000 cycles, the P_d value for the 1st cycle is 4960 W kg^{-1} and subjected to a drop up to 500th cycle with the average of 2277 W kg^{-1} and then continues constant with the average of 400 W kg^{-1} throughout the cycles beyond the 500th cycle. The drop of P_d at higher cycles is because of the depletion of the PE. Ion agglomeration after the fast charge-discharge mechanisms blocks the migration of ions to the electrodes that causes a decrease of adsorption of ions at the interfaces of the electrodes and PEs [79]. This tendency of P_d drop is in agreement with the rising

ESR tendency. The ESR raise at greater cycles due to the reduction in the mobile ion concentration and aggregation of ions after the swift processes of charge–discharge cycles offers smaller P_d at higher cycles [80]. The accomplished P_d for the EDLC cell is high in comparison to that reported in the literature (see ***Table 4***).

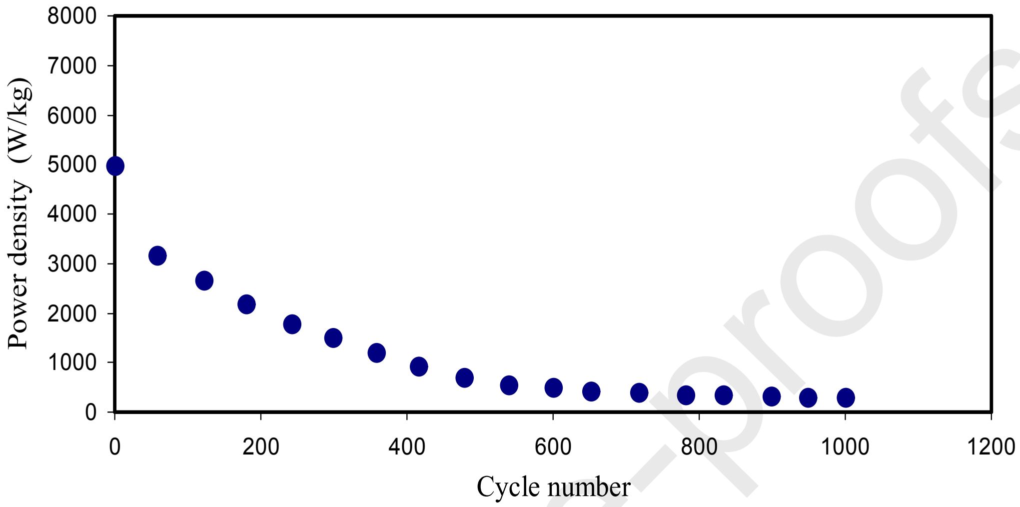

Figure 16. P_d of the developed EDLC for 1000 cycles.

4. Conclusion

PVA:NH$_4$SCN:Cu(II)-complex:GLY -based CPE was efficiently fabricated using the solution casting process. The addition of Cu(II)-complex and GLY maximized the σ_{DC} up to 2.25×10^{-3} Scm^{-1}. Outcome from the XRD route displayed that the highest glycerolized CPE exhibits the most amorphousity. Outcome from the XRD examination displayed that the utmost conducting plasticized system has the smallest degree of crystallinity and the XRD outcomes could also be associated to the trend in the degree of crystallinity with conductivity variation of the CPE sytems. Using the FTIR route, the interaction amongst PVA and the PE components was confirmed. The FESEM route revealed that the films surface morphology were smooth uniform at higher GLY concentration. TNM established that the dominant charge carriers were ions. The t_{ion} as well as t_{el} for the utmost conducting CPE were determined to be 0.971 and 0.029, respectively. LSV route displayed that the decomposition voltage for PGNC-4 system is at 2.15 V, suggesting its appropriateness in the EDLC application. Capacitive manner in the synthesized EDLC was confirmed by CV examination, as no redox peaks were perceived. C_{CV} was revealed to be affected by the used scan rates. The C_d and E_d of the EDLC are almost constant throughout 1000 cycles with average values of 155.322 F/g and 17.473 Wh/Kg, respectively at a current density of 0.5 mA/cm^2. Fortunately, the E_d of the EDLC in the current work is in the range of battery energy density. The low value of ESR indicates that the EDLC has a proper contact among the AC electrodes and the PEs. The EDLC has initial high P_d as 4960.31 W/Kg.

Acknowledgments

The authors appreciatively acknowledge the financial support for this work by the Ministry of Higher Education & Scientific Research-Kurdish National Research Council (KNRC).

Conflicts of Interest

The authors declare no conflict of interest.

References

[1] C.S. Lim, K.H. Teoh, C.W. Liew, S. Ramesh, Capacitive behavior studies on electrical double layer capacitor using poly (vinyl alcohol)-lithium perchlorate based polymer electrolyte incorporated with TiO2, Mater. Chem. Phys. 143 (2014) 661–667. https://doi.org/10.1016/j.matchemphys.2013.09.051

[2] M.A.A. Mohd Abdah, N.H.N. Azman, S. Kulandaivalu, Y. Sulaiman, Review of the use of transition-metal-oxide and conducting polymer-based fibres for high-performance supercapacitors, Mater. Des. 186 (2020) 108199. https://doi.org/10.1016/j.matdes.2019.108199.

[3] I. Hadjipaschalis, A. Poullikkas, V. Efthimiou, Overview of current and future energy storage technologies for electric power applications, Renew. Sustain. Energy Rev. 13 (2009) 1513–1522. https://doi.org/10.1016/j.rser.2008.09.028.

[4] M. Winter, R.J. Brodd, What are batteries, fuel cells, and supercapacitors?, Chem. Rev. 104 (2004) 4245–4269. https://doi.org/10.1021/cr020730k.

[5] M. Jayalakshmi, K. Balasubramanian, Simple capacitors to supercapacitors - An overview, Int. J. Electrochem. Sci. 3 (2008) 1196–1217. http://www.electrochemsci.org/papers/vol3/3111196.pdf.

[6] Y. Zhang, H. Feng, X. Wu, L. Wang, A. Zhang, T. Xia, H. Dong, X. Li, L. Zhang, Progress of electrochemical capacitor electrode materials: A review, Int. J. Hydrogen Energy. 34 (2009) 4889–4899. https://doi.org/10.1016/j.ijhydene.2009.04.005.

[7] S.N. Syahidah, S.R. Majid, Super-capacitive electro-chemical performance of polymer blend gel polymer electrolyte (GPE) in carbon-based electrical double-layer capacitors, Electrochim. Acta. 112 (2013) 678–685. https://doi.org/10.1016/j.electacta.2013.09.008.

[8] X.Y. Zhao, Y. Wu, J.P. Cao, Q.Q. Zhuang, X. Wan, S. He, X.Y. Wei, Preparation and characterization of activated carbons from oxygen-rich lignite for electric

double-layer capacitor, Int. J. Electrochem. Sci. 13 (2018) 2800–2816. https://doi.org/10.20964/2018.03.50.

[9] A.S.F.M. Asnawi, S.B. Aziz, M.M. Nofal, Y.M. Yusof, I. Brevik, M.H. Hamsan, M.A. Brza, R.T. Abdulwahid, M.F.Z. Kadir, Metal complex as a novel approach to enhance the amorphous phase and improve the EDLC performance of plasticized proton conducting chitosan-based polymer electrolyte, Membranes (Basel). 10 (2020) 1–20. https://doi.org/10.3390/membranes10060132.

[10] C. Shen. Lim, K. H. Teoh, H. M. Ng, C. -Wen Liew, S. Ramesh, Ionic conductivity enhancement studies of composite polymer electrolyte based on poly (vinyl alcohol)-lithium perchlorate-titanium oxide, Adv. Mater. Lett. 8 (2017) 465–471. https://doi.org/10.5185/amlett.2017.1410.

[11] Z. Wang, H. Li, Z. Tang, Z. Liu, Z. Ruan, L. Ma, Q. Yang, D. Wang, C. Zhi, Hydrogel Electrolytes for Flexible Aqueous Energy Storage Devices, Adv. Funct. Mater. 28 (2018) 1804560. https://doi.org/10.1002/adfm.201804560.

[12] J.P. Gong, Materials both tough and soft, Science. 344 (2014) 161–162. https://doi.org/10.1126/science.1252389.

[13] N.M. Saidi, F.S. Omar, A. Numan, D.C. Apperley, M.M. Algaradah, R. Kasi, A.J. Avestro, R.T. Subramaniam, Enhancing the Efficiency of a Dye-Sensitized Solar Cell Based on a Metal Oxide Nanocomposite Gel Polymer Electrolyte, ACS Appl. Mater. Interfaces. 11 (2019) 30185–30196. https://doi.org/10.1021/acsami.9b07062.

[14] S.B. Aziz, M.H. Hamsan, M.A. Brza, M.F.Z. Kadir, S.K. Muzakir, R.T. Abdulwahid, Effect of glycerol on EDLC characteristics of chitosan : methylcellulose polymer blend electrolytes, J. Mater. Res. Technol. 9 (2020) 8355–8366. https://doi.org/10.1016/j.jmrt.2020.05.114.

[15] M.Y. Chong, A. Numan, C.W. Liew, H.M. Ng, K. Ramesh, S. Ramesh, Enhancing the performance of green solid-state electric double-layer capacitor incorporated with fumed silica nanoparticles, J. Phys. Chem. Solids. 117 (2018) 194–203. https://doi.org/10.1016/j.jpcs.2018.02.030.

[16] J.M. Hadi, S.B. Aziz, M.S. Mustafa, M.H. Hamsan, R.T. Abdulwahid, M.F.Z. Kadir, H.O. Ghareeb, Role of nano-capacitor on dielectric constant enhancement in PEO:NH4SCN:xCeO2 polymer nano-composites: Electrical and electrochemical properties, J. Mater. Res. Technol. 9 (2020) 9283–9294. https://doi.org/10.1016/j.jmrt.2020.06.022.

[17] N. Farah, H.M. Ng, A. Numan, C.W. Liew, N.A.A. Latip, K. Ramesh, S. Ramesh, Solid polymer electrolytes based on poly(vinyl alcohol) incorporated with sodium salt and ionic liquid for electrical double layer capacitor, Mater. Sci. Eng. B Solid-State Mater. Adv. Technol. 251 (2019). https://doi.org/10.1016/j.mseb.2019.114468.

[18] S. B. Aziz, M. H. Hamsan, M. M. Nofal, S. San, R.T. Abdulwahid, S. Raza Saeed, M.A. Brza, M.F.Z. Kadir, S.J. Mohammed, S. Al-Zangana, From Cellulose, Shrimp and Crab Shells to Energy Storage EDLC Cells: The Study

of Structural and Electrochemical Properties of Proton Conducting Chitosan-Based Biopolymer Blend Electrolytes, Polymers (Basel). 12 (2020) 1526. https://doi.org/10.3390/polym12071526.

[19] S. Bashir, F.S. Omar, M. Hina, A. Numan, J. Iqbal, S. Ramesh, K. Ramesh, Synthesis and characterization of hybrid poly (N, N-dimethylacrylamide) composite hydrogel electrolytes and their performance in supercapacitor, Electrochim. Acta. 332 (2020) 135438. https://doi.org/10.1016/j.electacta.2019.135438.

[20] V. Saminatha Kumaran, H.M. Ng, S. Ramesh, K. Ramesh, B. Vengadaesvaran, A. Numan, The conductivity and dielectric studies of solid polymer electrolytes based on poly (acrylamide-co-acrylic acid) doped with sodium iodide, Ionics (Kiel). 24 (2018) 1947–1953. https://doi.org/10.1007/s11581-018-2448-z.

[21] X. Jiang, Y. Luo, L. Hou, Y. Zhao, The Effect of glycerol on the crystalline, thermal, and tensile properties of CaCl2-doped starch/PVA films, Polym. Compos. 37 (2015) 3191–3199. https://doi.org/10.1002/pc.23517.

[22] S. Peng, X. Jiang, X. Xiang, K. Chen, G. Chen, X. Jiang, L. Hou, High-performance and flexible solid-state supercapacitors based on high toughness and thermoplastic poly(vinyl alcohol)/NaCl/glycerol supramolecular gel polymer electrolyte, Electrochim. Acta. 324 (2019) 134874. https://doi.org/10.1016/j.electacta.2019.134874.

[23] K.A.M. Abd El-Kader, S.F. Abdel Hamied, A.B. Mansour, A.M.Y. El-Lawindy, F. El-Tantaway, Effect of the molecular weights on the optical and mechanical properties of poly(vinyl alcohol) films, Polym. Test. 21 (2002) 847–850. https://doi.org/10.1016/S0142-9418(02)00020-X.

[24] N. Srivastava, A. Chandra, S. Chandra, Dense branched growth of (SCN)x and ion transport in the poly(ethyleneoxide) NH4SCN polymer electrolyte, Phys. Rev. B. 52 (1995) 225. https://doi.org/10.1103/PhysRevB.52.225.

[25] H.D.B. Jenkins, D.F.C. Morris, A new estimation of the lattice energies of the ammonium halides and the proton affinity of gaseous ammonia, Mol. Phys. 32 (1976) 231–236. https://doi.org/10.1080/00268977600101741.

[26] Kadir, M. F. Z, Characteristics of proton conducting PVA-chitosan polymer blend electrolytes. Doctoral Dissertation University of Malaya (2010). Kuala Lumpur, Malaysia.

[27] M.F. Shukur, M.F.Z. Kadir, Electrical and transport properties of NH4Br-doped cornstarch-based solid biopolymer electrolyte, Ionics (Kiel). 21 (2014) 111–124. https://doi.org/10.1007/s11581-014-1157-5.

[28] M.F. Shukur, M.F.Z. Kadir, Hydrogen ion conducting starch-chitosan blend based electrolyte for application in electrochemical devices, Electrochim. Acta. 158 (2015) 152–165. https://doi.org/10.1016/j.electacta.2015.01.167.

[29] M.A. Brza, S.B. Aziz, H. Anuar, M.H.F. Al Hazza, From green remediation to polymer hybrid fabrication with improved optical band gaps, Int. J. Mol. Sci. 20 (2019) 3910. https://doi.org/10.3390/ijms20163910.

[30] A.A. Mohamad, A.K. Arof, Plasticized alkaline solid polymer electrolyte system, Mater. Lett. 61 (2007) 3096–3099. https://doi.org/10.1016/j.matlet.2006.11.030.

[31] S. Ramesh, C.W. Liew, K. Ramesh, Evaluation and investigation on the effect of ionic liquid onto PMMA-PVC gel polymer blend electrolytes, J. Non. Cryst. Solids. 357 (2011) 2132–2138. https://doi.org/10.1016/j.jnoncrysol.2011.03.004.

[32] A.S.F.M. Asnawi, S.B. Aziz, M.M. Nofal, M.H. Hamsan, M.A. Brza, Y.M. Yusof, R.T. Abdilwahid, S.K. Muzakir, M.F.Z. Kadir, Glycerolized Li+ ion conducting chitosan-based polymer electrolyte for energy storage EDLC device applications with relatively high energy density, Polymers (Basel). 12 (2020) 1–19. https://doi.org/10.3390/polym12061433.

[33] M. Hema, S. Selvasekerapandian, A. Sakunthala, D. Arunkumar, H. Nithya, Structural, vibrational and electrical characterization of PVA-NH4Br polymer electrolyte system, Phys. B Condens. Matter. 403 (2008) 2740–2747. https://doi.org/10.1016/j.physb.2008.02.001.

[34] R. Hemalatha, M. Alagar, S. Selvasekarapandian, B. Sundaresan, V. Moniha, Studies of proton conducting polymer electrolyte based on PVA, amino acid proline and NH4SCN, J. Sci. Adv. Mater. Devices. 4 (2019) 101–110. https://doi.org/10.1016/j.jsamd.2019.01.004.

[35] S.B. Aziz, M.A. Rasheed, A.M. Hussein, H.M. Ahmed, Fabrication of polymer blend composites based on [PVA-PVP](1−x):(Ag2S)x ($0.01 \leq x \leq 0.03$) with small optical band gaps: Structural and optical properties, Mater. Sci. Semicond. Process. 71 (2017) 197–203. https://doi.org/10.1016/j.mssp.2017.05.035.

[36] S.B. Aziz, Modifying Poly(Vinyl Alcohol) (PVA) from Insulator to Small-Bandgap Polymer: A Novel Approach for Organic Solar Cells and Optoelectronic Devices, J. Electron. Mater. 45 (2016) 736–745. https://doi.org/10.1007/s11664-015-4191-9.

[37] N.N.A. Amran, N.S.A. Manan, M.F.Z. Kadir, The effect of LiCF3SO3 on the complexation with potato starch-chitosan blend polymer electrolytes, Ionics (Kiel). 22 (2016) 1647–1658. https://doi.org/10.1007/s11581-016-1684-3.

[38] N. A. M. Noor, M.I.N. Isa, Structural and Conduction Studies of Solid Biopolymer Electrolytes System Based on Carboxymethyl Cellulose, Am. J. Sustain. Agric. 9 (2015) 15–22.

[39] N. S. Salleh, S. B. Aziz, Z. Aspanut, M. F. Z. Kadir, Electrical impedance and conduction mechanism analysis of biopolymer electrolytes based on methyl cellulose doped with ammonium iodide, Ionics, 22 (2016), 2157–2167. doi:10.1007/s11581-016-1731-0

[40] S. Liang, Q. Huang, L. Liu, K.I. Yam, Microstructure and molecular interaction in glycerol plasticized chitosan/poly (vinyl alcohol) blending films, Macromol. Chem. Phys. 210 (2009) 832–839. https://doi.org/10.1002/macp.200900053.

[41] M.H. Makled, E. Sheha, T.S. Shanap, M.K. El-Mansy, Electrical conduction and dielectric relaxation in p-type PVA/CuI polymer composite, J. Adv. Res. 4 (2013) 531–538. https://doi.org/10.1016/j.jare.2012.09.007.

[42] A. Kharazmi, N. Faraji, R.M. Hussin, E. Saion, W.M.M. Yunus, K. Behzad, Structural, optical, opto-thermal and thermal properties of ZnS-PVA nanofluids synthesized through a radiolytic approach, Beilstein J. Nanotechnol. 6 (2015) 529–536. https://doi.org/10.3762/bjnano.6.55.

[43] L. Jiang, T. Yang, L. Peng, Y. Dan, Acrylamide modified poly(vinyl alcohol): Crystalline and enhanced water solubility, RSC Adv. 5 (2015) 86598–86605. https://doi.org/10.1039/c5ra18437a.

[44] S.B. Aziz, M.F.Z. Kadir, M.H. Hamsan, H.J. Woo, M.A. Brza, Development of Polymer Blends Based on PVA:POZ with Low Dielectric Constant for Microelectronic Applications, Sci. Rep. 9 (2019) 1–12. https://doi.org/10.1038/s41598-019-49715-8.

[45] N.N. Mobarak, A. Ahmad, M.P. Abdullah, N. Ramli, M.Y.A. Rahman, Conductivity enhancement via chemical modification of chitosan based green polymer electrolyte, Electrochim. Acta. 92 (2013) 161–167. https://doi.org/10.1016/j.electacta.2012.12.126.

[46] M.H. Hamsan, M.F. Shukur, M.F.Z. Kadir, NH4NO3 as charge carrier contributor in glycerolized potato starch-methyl cellulose blend-based polymer electrolyte and the application in electrochemical double-layer capacitor, Ionics (Kiel). 23 (2017) 3429–3453. https://doi.org/10.1007/s11581-017-2155-1.

[47] M.R. Johan, L.M. Ting, Structural, thermal and electrical properties of nano manganese-composite polymer electrolytes, Int. J. Electrochem. Sci. 6 (2011) 4737–4748.

[48] S.B. Aziz, Morphological and optical characteristics of chitosan(1−x):Cuox (4 ≤ x ≤ 12) based polymer nano-composites: Optical dielectric loss as an alternative method for tauc's model, Nanomaterials. 7 (2017) 1–15. https://doi.org/10.3390/nano7120444.

[49] M.F.Z. Kadir, N.S. Salleh, M.H. Hamsan, Z. Aspanut, N.A. Majid, M.F. Shukur, Biopolymeric electrolyte based on glycerolized methyl cellulose with NH4Br as proton source and potential application in EDLC, Ionics (Kiel). 24 (2018) 1651–1662. https://doi.org/10.1007/s11581-017-2330-4.

[50] S. Cho, C. F. Chen, P.P. Mukherjee, Influence of Microstructure on Impedance Response in Intercalation Electrodes, J. Electrochem. Soc. 162 (2015) A1202–A1214. https://doi.org/10.1149/2.0331507jes.

[51] A.M. Svensson, L.O. Valøen, R. Tunold, Modeling of the impedance response of porous metal hydride electrodes, Electrochim. Acta. 50 (2005) 2647–2653. https://doi.org/10.1016/j.electacta.2004.11.035.

[52] S.B. Aziz, Z.H.Z. Abidin, A.K. Arof, Influence of silver ion reduction on electrical modulus parameters of solid polymer electrolyte based on chitosan-silver triflate electrolyte membrane, Express Polym. Lett. 4 (2010) 300–310. https://doi.org/10.3144/expresspolymlett.2010.38.

[53] D.K. Pradhan, B.K. Samantaray, R.N.P. Choudhary, N.K. Karan, R. Thomas, R.S. Katiyar, Effect of plasticizer on structural and electrical properties of nanocomposite solid polymer electrolytes, Ionics (Kiel). 17 (2011) 127–134. https://doi.org/10.1007/s11581-010-0491-5.

[54] S.B. Aziz, R.M. Abdullah, Crystalline and amorphous phase identification from the tanδ relaxation peaks and impedance plots in polymer blend electrolytes based on [CS:AgNt]x:PEO(x-1) ($10 \leq x \leq 50$), Electrochim. Acta. 285 (2018) 30–46. https://doi.org/10.1016/j.electacta.2018.07.233.

[55] V.S. Rangasamy, S. Thayumanasundaram, J.P. Locquet, Solid polymer electrolytes with poly(vinyl alcohol) and piperidinium based ionic liquid for Li-ion batteries, Solid State Ionics. 333 (2019) 76–82. https://doi.org/10.1016/j.ssi.2019.01.024.

[56] C.W. Liew, Nanocomposite Polymer Electrolytes for Electric Double Layer Capacitors (EDLCs) Application, in: Nanomaterials in energy devices, by J.H. Kiat (Ed.), First Ed., CRC Press Taylor & Francis Group, 2017: p. 40.

[57] S.B. Aziz, M.H. Hamsan, M.A. Brza, M.F.Z. Kadir, R.T. Abdulwahid, H.O. Ghareeb, H.J. Woo, Fabrication of energy storage EDLC device based on CS:PEO polymer blend electrolytes with high Li+ ion transference number, Results Phys. 15 (2019) 102584. https://doi.org/10.1016/j.rinp.2019.102584.

[58] S.B. Aziz, Li+ ion conduction mechanism in poly (ε-caprolactone)-based polymer electrolyte, Iran. Polym. J. 22 (2013) 877–883. https://doi.org/10.1007/s13726-013-0186-7.

[59] N.K. Zainuddin, N.M.J. Rasali, N.F. Mazuki, M.A. Saadiah, A.S. Samsudin, Investigation on favourable ionic conduction based on CMC-K carrageenan proton conducting hybrid solid bio-polymer electrolytes for applications in EDLC, Int. J. Hydrogen Energy. 45 (2020) 8727–8741. https://doi.org/10.1016/j.ijhydene.2020.01.038.

[60] A.K. Arof, S.R. Majid, Electrical Studies on Chitosan Based Proton Conductors and Application in Capacitors, Mol. Cryst. Liq. Cryst. 484 (2008) 107/[473]-116/[482]. https://doi.org/10.1080/15421400801904245.

[61] M.H. Hamsan, M.F. Shukur, S.B. Aziz, Y.M. Yusof, M.F.Z. Kadir, Influence of NH4Br as an ionic source on the structural/electrical properties of dextran-based biopolymer electrolytes and EDLC application, Bull. Mater. Sci. 43 (2020). https://doi.org/10.1007/s12034-019-2008-9.

[62] M.F.Z. Kadir, A.K. Arof, Application of PVA-chitosan blend polymer electrolyte membrane in electrical double layer capacitor, Mater. Res. Innov. 15 (2011) s217–s220. https://doi.org/10.1179/143307511X13031890749299.

[63] C.W. Liew, S. Ramesh, A.K. Arof, Characterization of ionic liquid added poly(vinyl alcohol)-based proton conducting polymer electrolytes and electrochemical studies on the supercapacitors, Int. J. Hydrogen Energy. 40 (2015) 852–862. https://doi.org/10.1016/j.ijhydene.2014.09.160.

[64] S.B. Aziz, M.A. Brza, M.H. Hamsan, M.F.Z. Kadir, S.K. Muzakir, R.T. Abdulwahid, Effect of ohmic-drop on electrochemical performance of EDLC fabricated from PVA: Dextran: NH4I based polymer blend electrolytes, J. Mater. Res. Technol. 9 (2020) 3734–3745. https://doi.org/10.1016/j.jmrt.2020.01.110.

[65] N.E.A. Shuhaimi, L.P. Teo, H.J. Woo, S.R. Majid, A.K. Arof, Electrical double-layer capacitors with plasticized polymer electrolyte based on methyl cellulose, Polym. Bull. 69 (2012) 807–826. https://doi.org/10.1007/s00289-012-0763-5.

[66] S.B. Aziz, M.A. Brza, K. Mishra, M.H. Hamsan, W.O. Karim, R.M. Abdullah, M.F.Z. Kadir, R.T. Abdulwahid, Fabrication of high performance energy storage EDLC device from proton conducting methylcellulose: Dextran polymer blend electrolytes, J. Mater. Res. Technol. 9 (2020) 1137–1150. https://doi.org/10.1016/j.jmrt.2019.11.042.

[67] M. Selvakumar, D.K. Bhat, LiClO4 Doped Cellulose Acetate as Biodegradable Polymer Electrolyte for Supercapacitors, J. Appl. Polym. Sci. 110 (2008) 594–602. https://doi.org/10.1002/app.28671.

[68] J. Lee, W. Kim, W. Kim, Stretchable carbon nanotube/ion-gel supercapacitors with high durability realized through interfacial microroughness, ACS Appl. Mater. Interfaces. 6 (2014) 13578–13586. https://doi.org/10.1021/am502953g.

[69] M.S.A. Rani, A. Ahmad, N.S. Mohamed, Influence of nano-sized fumed silica on physicochemical and electrochemical properties of cellulose derivatives-ionic liquid biopolymer electrolytes, Ionics (Kiel). 24 (2018) 807–814. https://doi.org/10.1007/s11581-017-2235-2.

[70] G.P. Pandey, Y. Kumar, S.A. Hashmi, Ionic liquid incorporated polymer electrolytes for supercapacitor application, Indian J. Chem. 49 (2010) 743–751.

[71] R. Pratap, B. Singh, S. Chandra, Polymeric rechargeable solid-state proton battery, J. Power Sources. 161 (2006) 702–706. https://doi.org/10.1016/j.jpowsour.2006.04.020.

[72] C. Liew, S. Ramesh, Electrical, structural, thermal and electrochemical properties of corn starch-based biopolymer electrolytes, Carbohydr. Polym. 124 (2015) 222–228. https://doi.org/10.1016/j.carbpol.2015.02.024.

[73] C. Lim, K.H. Teoh, C. Liew, S. Ramesh, Electric double layer capacitor based on activated carbon electrode and biodegradable composite polymer electrolyte, Ionics (Kiel). 20 (2014) 251–258. https://doi.org/10.1007/s11581-013-0982-2.

[74] L. Fan, M. Wang, Z. Zhang, G. Qin, X. Hu, Q. Chen, Preparation and characterization of PVA alkaline solid polymer electrolyte with addition of bamboo charcoal, Materials (Basel). 11 (2018) 679. https://doi.org/10.3390/ma11050679.

[75] A.K. Arof, M.Z. Kufian, M.F. Syukur, M.F. Aziz, A.E. Abdelrahman, S.R. Majid, Electrical double layer capacitor using poly (methyl methacrylate)–C4BO8Li gel polymer electrolyte and carbonaceous material from shells of mata kucing (Dimocarpus longan) fruit, Electrochim. Acta. 74 (2012) 39–45. https://doi.org/10.1016/j.electacta.2012.03.171.

[76] S.N. Asmara, M.Z. Kufian, S.R. Majid, A.K. Arof, Preparation and characterization of magnesium ion gel polymer electrolytes for application in electrical double layer capacitors, Electrochim. Acta. 57 (2011) 91–97. https://doi.org/10.1016/j.electacta.2011.06.045.

[77] M.S. Kumar, D.K. Bhat, Polyvinyl alcohol – polystyrene sulphonic acid blend electrolyte for supercapacitor application, Phys. B Condens. Matter. 404 (2009) 1143–1147. https://doi.org/10.1016/j.physb.2008.11.072.

[78] Y.Z. Wei, B. Fang, S. Iwasa, M. Kumagai, A novel electrode material for electric double-layer capacitors, J. Power Sources. 141 (2005) 386–391. https://doi.org/10.1016/j.jpowsour.2004.10.001.

[79] C. Liew, S. Ramesh, A.K. Arof, Enhanced capacitance of EDLCs (electrical double layer capacitors) based on ionic liquid-added polymer electrolytes, Energy. 109 (2016) 546–556. https://doi.org/10.1016/j.energy.2016.05.019.

[80] C. Zhong, Y. Deng, W. Hu, J. Qiao, L. Zhang, J. Zhang, A review of electrolyte materials and compositions for electrochemical supercapacitors, Chem. Soc. Rev. 44 (2015) 7484–7539. https://doi.org/10.1039/c5cs00303b.

Author agreement

All authors agree to submit and publish this work. The article has been written by the stated authors who are ALL aware of its content and approve its submission.